Investigating the Effect of Energy Dissipation on Flotation Kinetics in an Oscillating Grid Flotation Cell

by

Wesley Thomas Massey
B.Sc. Chemical Engineering (University of Cape Town)

Thesis Presented for the Degree of
MASTER OF SCIENCE IN ENGINEERING

Department of Chemical Engineering
University of Cape Town
November 2011

Declaration

I know the meaning of plagiarism and declare that all the work in the document, save for that which is properly acknowledged, is my own

---

Wesley Massey
28th November, 2011

Acknowledgements

I would like to sincerely thank my supervisor, Professor David Deglon, and co-supervisor, Martin Harris, for their guidance, constant support and good humour, which is very much appreciated.

The following institutions and people are gratefully acknowledged:

- The AMIRA P9O project for funding this research.
- Peter Dobias, Joachim Macke, Bill Randall and Granville de la Cruz for the construction of the apparatus used in this study.
- Jenny Wiese and Kenneth Maseko for their assistance during my time in the laboratory.
- All of the staff and students at the Centre for Minerals Research for their assistance and making my time there a thoroughly enjoyable experience.
- Heather Sundström for her assistance with my numerous administrative and purchasing issues.
- My parents and my girlfriend, Claire, for their unwavering patience, support and encouragement.

Synopsis

This thesis investigates the effect of energy dissipation on the flotation kinetics of quartz in an oscillating grid flotation cell. Oscillating grids exhibit relatively isotropic and homogeneous turbulence, which cannot be achieved in standard impeller agitated flotation cells. Due to this they provide a potentially ideal environment in which to investigate the effects of energy dissipation on flotation kinetics. Previous work in an oscillating grid flotation cell was limited to energy dissipations of up to 0.6 kW/m^3, which is low when compared to 0.6 – 3 kW/m^3 commonly used in both flotation literature and industry.

The current work uses a new oscillating grid cell which can operate at energy dissipations of up to 5 kW/m^3. Quartz (sub 100 μm) has been floated in the new cell at energy dissipations ranging from 0.5 – 5 kW/m^3 and using three discrete bubble sizes (0.13 mm, 0.24 mm and 0.82 mm). Characterisation experiments show that the new cell operates in a similar manner to the oscillating grid cell used by Changunda et al. (2008), and produces repeatable results. The effect of changing bubble and particle size on flotation kinetics is in agreement with literature findings, indicating that as a flotation device the oscillating grid cell is operating as expected.

Results from the flotation experiments show that the effect of energy dissipation on flotation kinetics is strongly dependent on both particle and bubble size. The highest flotation rates, for all particle sizes, are achieved when floating with fine bubbles at low energy dissipations. For flotation with fine bubbles, increasing the energy dissipation results in the flotation rates for fine particles remaining constant, and the flotation rates for coarse particles decreasing. When floating with larger bubbles, near the size typically found in industry, increasing the energy dissipation is beneficial for the flotation of both intermediate and fine particles, with fine particles benefiting the most from increased energy dissipation. For the flotation of more coarse parti-

cles, increasing energy dissipation is beneficial to an optimum point, beyond which increasing energy dissipation results in decreased flotation rates. The value of this optimum energy dissipation decreases with decreasing bubble size.

Higher flotation rates with increased energy dissipation are thought to occur due to increased collision frequencies between particles and bubbles. Increasing energy dissipation may also lead to increased detachment of particles from bubbles, which may account for decreasing flotation rates with increased energy dissipation. From the results, it would appear that detachment rates increased with decreasing bubble size and increasing particles size.

The relationship between flotation rate and energy dissipation, in conditions where detachment is thought to be negligible, can be described by the relationship $k \propto \epsilon^{0.7-0.9}$. This relationship is stronger than theory would suggest, and is in agreement with literature experimental studies which have made similar observations.

The results are compared with results from literature studies which used an oscillatory baffled column and a stirred cell, in order to investigate the effect of contacting environment on flotation kinetics. At low energy dissipation the results from the oscillating grid cell and the stirred cell are similar, whilst they deviate at higher energy dissipations. This observation is possibly due to high levels of detachment in the impeller zone of the stirred cell. The results in this study for the effect of energy dissipation on flotation kinetics may, therefore, be considered to be a more accurate representation than experimental studies conducted in stirred cells.

Contents

List of Figures

List of Tables

Nomenclature

Latin Letters

A	Constant in attachment efficiency model	
a	Acceleration in an turbulent environment	$m.s^{-2}$
B	Constant in attachment efficiency model	
C_d	Drag coefficient	
d_b	Bubble diameter	m
d_p	Particle diameter	m
E_1	Surface energy barrier	J
E_a	Efficiency of attachment	
E_{coll}	Efficiency of collection	
E_c	Efficiency of collision	
$E_{k\text{-}A}$	Kinetic energy of attachment	J
$E_{k\text{-}D}$	Kinetic energy of detachment	J
E_s	Efficiency of stability	
F	Force	N
f	Oscillating frequency	Hz
F_{det}	Forces of detachment	N
G	Shear rate of a fluid	s^{-1}
g	Acceleration due to gravity	$m.s^{-2}$
H	Cell height	m
h	Distance from a grid	m
k	First order flotation rate constant	s^{-1} or min^{-1}
K_3	Dimensionless number in generalised Sutherland equation	

M	Grid mesh spacing	m
m_b	Bubble mass	kg
m_L	Mass of liquid being agitated	kg
m_p	Particle mass	kg
n	Number of grids	
N_b	Number of bubbles per unit volume	m^{-3}
N_p	Number of particles per unit volume	m^{-3}
P	Power	W
Q	Gas volumetric flowrate	$m^3.s^{-1}$
R	Recovery	
r	Radius	m
Re_b	Reynolds number	
S	Stroke length	m
St	Stokes number	
T	Tenacity of attachment	N
t	Time	s
t_{ind}	Induction time	s
TKE	Total kinematic energy of turbulence	$m^2.s^{-2}$
u'	Root mean square (RMS) fluctuating velocity	$m.s^{-1}$
V_c	Cell volume	m^3
v_b	Rise velocity of a bubble in stationary fluid	$m.s^{-1}$
v_b'	Velocity of a bubble in shearing fluid	$m.s^{-1}$
W_A	Work of adhesion	J
$\ddot{Y}$	Acceleration in oscillating system	$m.s^{-2}$
$\dot{Y}$	Velocity in oscillating system	$m.s^{-1}$
Y	Displacement in oscillating system	m
Z	Rate of collision per unit volume	$m^{-3}.s^{-1}$

Greek Letters

β	Dimensionless number in generalised Sutherland equation	
$\overline{\epsilon}$	Mean energy dissipation rate	$m^2.s^{-3}$ or $kW.m^{-3}$ or $W.kg^{-1}$

ϵ	Energy dissipation rate	$m^2.s^{-3}$ or $kW.m^{-3}$ or $W.kg^{-1}$
Λ	Macro scale of turbulence	m
λ	Turbulent eddy scale	m
ν	Kinematic viscosity	$m^2.s^{-1}$
η	Kolmogorov micro scale of turbulence	m
ϕ	Angle of capillary force	rad
ρ	Density	$kg.m^{-3}$
σ	Surface tension	N/m
τ	Period of oscillation	s
τ_k	Kolmogorov time scale	s
$\tau_{p/b}$	Particle/bubble relaxation time	s
θ	Particle contact angle	degrees
θ_a	Adhesion angle	degrees
θ_t	Angle of tangency in generalised Sutherland equation	degrees
μ_f	Viscosity	Pa.s
ω	Angular velocity of microscale eddy	$rad.s^{-1}$
ω_{imp}	Angular velocity of an impeller	$rad.s^{-1}$

Subscripts

a	Attachment
b	Bubble
f	Fluid
c	Collision
p	Particles
s	Stability

Chapter 1

Introduction

Froth flotation is a process which is used extensively in the mining industry for the beneficiation of ore, treating an estimated two billion tons of ores and coal annually (Nguyen and Schulze, 2004). Due to the extensive use industrially, any inefficiencies in flotation can lead to large losses in revenue. As more low grade, finely disseminated ore bodies are mined flotation faces rising challenges. There is therefore an increased demand on knowledge and understanding of flotation in order to increase the efficiency of the process.

Knowledge of the effect of energy dissipation on flotation kinetics is a potentially important factor in areas such as the optimisation of installed plants, the design of new plants and the design of new flotation machines. Historically the investigations into the effect of energy dissipation on flotation kinetics have been carried out in Rushton impeller stirred cells, sparged with bubbles of a known size (Ahmed and Jameson, 1985; Deglon, 1998; Pyke et al., 2003; Sherrell, 2004; Newell and Grano, 2006). Investigations using this type of cell have limitations due to the fact that the impeller influences the particle suspension, bubble break-up and agitation in the system. Additionally the turbulence is highly inhomogeneous and anisotropic, with energy dissipation rates near the impeller which are 5 – 200 times those found elsewhere in the cell (Schubert, 2008).

These limitations have resulted in the development of novel cells for the investigation of energy dissipation. Anderson (2008) developed a novel oscillatory baffled column which had the benefit of decoupling solid suspension, bubble generation and

energy dissipation in a more homogeneous turbulent environment. It was found that the unique bulk oscillatory motion of the fluid in the cell had a very strong effect on the flotation kinetics at very low energy dissipations. This cell has potential in industrial applications due to the increase in flotation kinetics at relatively low energy dissipations. However as a research tool it is not ideal due to the complex nature of the flow which differs highly from a conventional stirred cell.

Changunda et al. (2008) used a novel oscillating grid cell, based on the design of Bache and Rasool (2001), to investigate the effects of energy dissipation on flotation kinetics. The oscillating grid cell decouples the processes of particle suspension and bubble generation as well as producing relatively homogeneous, isotropic turbulence with zero mean flow. Due to the near ideal nature of the turbulence generated, oscillating grids have been used in many areas of research including combustion (DeSilva and Fernando, 1994), resuspension (Orlins and Gulliver, 2003), sedimentation (Huppert et al., 1995), mixing across density layers (McDougall, 1979), coagulation (Brunk et al., 1998) and precipitation (Mokgethi, 2010).

The oscillating grid cell used by Changunda et al. (2008) was a proof of concept device and was limited to energy dissipations of less than 0.6 kW/m^3. This is low compared to energy dissipations of 1 – 3 kW/m^3 commonly used in industrial applications (Deglon et al., 2000). The study was conducted on quartz, methylated to an advancing contact angle of 65°, floated with three discrete bubble sizes (0.13 mm, 0.24 mm and 0.82 mm). Experiments at low energy dissipation showed that the oscillating grid cell performed in a similar manner to conventional stirred cells with regard to the effects of bubble and particle size. It was found that increasing the energy dissipation in the system resulted in the flotation rates increasing linearly for all particle and bubble sizes used.

1.1 Objectives of Thesis

From the results of Changunda et al. (2008), the oscillating grid cell was considered to potentially be an ideal tool for the research of flotation kinetics in turbulent systems. The objective of the current study was therefore to investigate the effect of energy dissipation on flotation kinetics in an oscillating grid cell, over a larger range of energy

dissipations, including those commonly used in industry. The project was composed of three parts which were carried out to achieve the objective:

- A new oscillating grid cell was designed and built with a more robust design than that used by Changunda et al. (2008), such that the desired energy dissipations could be achieved. The new cell operated in batch mode and could produce discrete bubble sizes independently of the energy dissipation.
- Flotation of methylated quartz was performed using the same operating conditions and methylated quartz as Changunda et al. (2008) in order to benchmark the cell against the results of that study.
- Natural quartz flotation experiments were conducted in the oscillating grid cell at energy dissipations of 0.5 – 5 kW/m^3. The energy dissipations used were chosen to cover a large range, including the dissipations which may be of interest to industry. Conditions were chosen so as to make the results comparable to studies in an oscillatory baffled column (Anderson, 2008) and a stirred cell (Deglon, 1998). These experiments allowed observations to be made on the effect of energy dissipation on flotation kinetics as well as the role of particle and bubble size. Additionally the role of the contacting environment could be investigated.

1.2 Scope and Limitations

In this thesis the single mineral flotation of fine quartz is investigated in an oscillating grid cell. Quartz is used as it is a literature standard, and so as to make the results comparable to studies in an oscillatory baffled column (Anderson, 2008) and a stirred cell (Deglon, 1998). The investigation is limited to the pulp phase of the flotation of a single density and single hydrophobicity ore.

Chapter 2

Literature Review

In this chapter the relevant literature regarding flotation and oscillating grids will be reviewed, for both theoretical and experimental studies. In order to set the scene for this project the various types of flotation cells used in industrial applications, and novel flotation cells, are briefly reviewed in Section 2.1. Turbulence fundamentals are briefly discussed in Section 2.2 with a focus on elements relevant to flotation processes. The characteristics of oscillating grid turbulence are then reviewed in Section 2.3. The fundamental theories of flotation in turbulent systems are reviewed in Section 2.4, along with models which describe them. There have been numerous experimental studies on flotation, which are briefly reviewed in Section 2.5 with a focus on the effects of bubble size, particle size and energy dissipation on flotation kinetics.

2.1 Flotation Cells

There are three primary functions that a flotation cell preforms, namely, particle suspension, bubble break-up and particle-bubble contacting. The most common types of flotation cells used in industry are mechanical cells and, to a lesser extent, column cells. In addition to these cells there are numerous novel cells which have been developed. This section will outline some of the different cells used, and briefly discuss the benefits and limitations of each.

2.1.1 Mechanical Flotation Cells

Mechanical, or conventional, flotation cells are the most commonly used cells in industry, and are considered as the industry standard. They utilise an impeller for the functions of particle suspension, bubble break-up and particle-bubble contacting. The volume of such cells may vary from 2 L for laboratory use, to up to 350 m^3 in industry. Recent developments in mechanical cell design have typically centred around the use of larger cells, a trend which is driven by the economic benefits of using larger equipment. The metallurgical effects of using large cells are not fully understood, however there is evidence to suggest that cell size may be increased without loss of metallurgical performance (Yianatos et al., 2008). The typical energy dissipation used in industrial mechanical cells ranges from 0.6 – 3 kW/m^3 (Deglon et al., 2000; Lelinski et al., 2011). A typical modern mechanical cell is depicted in Figure 2.1.

Figure 2.1: Schematic of a modern day mechanical flotation cell (FLSmidth SuperCell^{TM}).

Mechanical cells have an inherently inhomogeneous distribution of energy dissipation through the cell, with high energy dissipation levels found near the impeller and much lower levels in the bulk of the cell (Deglon, 1998; Koh and Schwarz, 2003; Newell and Grano, 2007; Schubert, 2008). The fact that the processes of particle suspension, bubble break-up and energy generation are all interdependent make it difficult or impossible to optimise the conditions for flotation (Schubert, 1999, 2008).

2.1.2 Column Flotation Cells

Column flotation cells are used industrially, though to a lesser extent than mechanical cells. A schematic of a column flotation cell is shown in Figure 2.2.

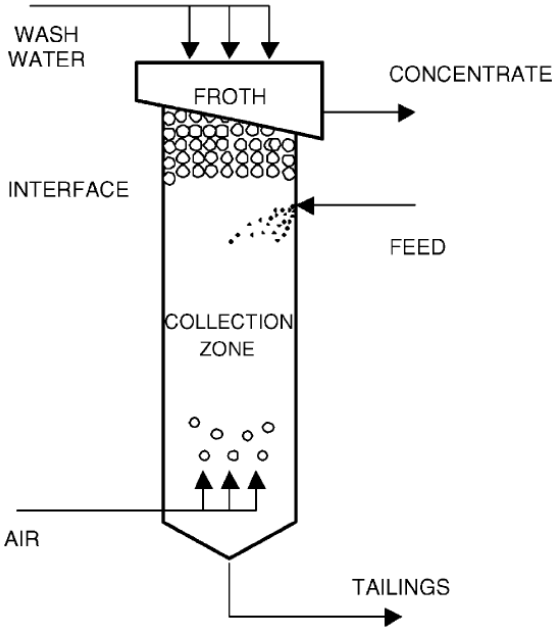

Figure 2.2: Schematic of a column flotation cell (from Bergh and Yianatos, 2003).

Column cells operate by introducing ore near the top of the column and sparging air from the bottom. This produces a counter-current flow in the collection zone, which promotes particle-bubble contacting. Industrially these cells are operated with deep froths of approximately 1 m, which have wash water added, aiding in the removal of entrained fine particles (Bergh and Yianatos, 2003). Columns typically yield higher concentrate grades than mechanical cells and are therefore generally used as cleaners. Column cells are poor for floating small, light particles since there is no added energy dissipation, and the particles therefore rely on their own inertia to break through the streamlines around the bubbles.

2.1.3 Novel Flotation Cells

Much of the development of new flotation technologies has centered around the generation of small bubbles and the development of reactor/separator type cells. Fine bubble generation has been developed through methods such as improved sparger design, dissolved air flotation and electroflotation. Reviews on these subjects can be found in Finch (1995), Rodrigues and Rubio (2007) and Miettinen et al. (2010). This section will review some novel cells which provide alternative turbulent environments for flotation.

2.1.3.1 Reactor/Separator Cells

There are multiple examples of reactor/separator type cells (Finch, 1995), though possibly the best known cell is the Jameson cell. A schematic of a Jameson cell is shown in Figure 2.3.

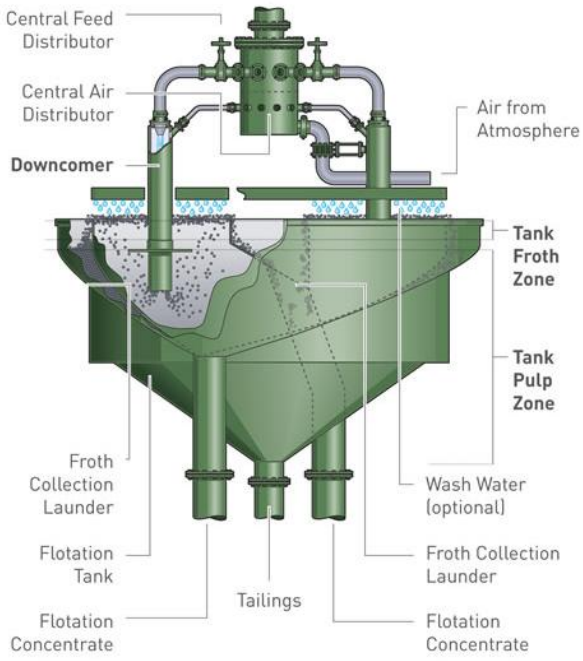

Figure 2.3: Schematic of a Jameson flotation cell (Xtrata Jameson Cell).

The concept of the reactor/separator type cell is to separate the processes of particle-bubble contacting and the removal of the particle-bubble aggregates from the pulp.

This is generally achieved by mixing the bubbles and slurry in a vertical downcomer which supplies the turbulence for contacting. The downcomer then discharges into a quiescent zone where the aggregates are allowed to rise to the surface. This separation of the contacting and separation allows for each to be independently optimised.

2.1.3.2 Agitated Columns

The agitated column is a concept which was developed to aid the flotation of fine particles in column cells, through adding turbulence to a standard column cell. Breytenbach (1995) developed an agitated column by added four impellers down the length of a flotation column. It was found that quartz flotation rates could be increased substantially over a standard column cell, and that fine particle (sub 40 μm) recoveries were superior to those in a standard batch cell and a Jameson cell. Ityokumbul et al. (2000) tested the same design on the flotation of pyrite with a particle size of 62 % passing 25 μm. It was found that the recovery of pyrite increased with increasing energy dissipation, however above 0.3 kW/m^3 the grade decreased sharply.

The oscillatory baffled column (Anderson, 2008) is a design which produces turbulence in a column through an unique oscillatory flow. Experiments floating sub 100 μm quartz found that the flotation rates could be greatly increased with low increases in energy dissipations of up to 0.05 kW/m^3. An attribute of the oscillatory flow was that the flotation rate could be increased 1.4 to 1.6 fold over a conventional column, regardless of the fluid viscosity. It was therefore speculated that this device shows potential for the flotation of viscous, non-Newtonian slurries. This cell is discussed in more detail in Section 2.5.3.

2.1.3.3 Recent Novel Cells

Jameson (2010) proposed two new flotation devices. The first is the Concorde cell, which operates by forcing pressurised, aerated slurry through a choke into an open cell, creating a supersonic shockwave. This shockwave is reported to produce very high energy dissipations in the order of 100 kW/m^3. Experimental results in PGM flotation (P_{80} = 53 μm) have indicated that the cell produces substantially increased flotation rates over conventional cells.

The second device proposed by Jameson (2010) is the fluidised bed flotation cell, which is focused on coarse particle flotation. The fluidised bed concept aims at producing high levels of contacting at low energy dissipations, so as to minimise the detachment of coarse particles. This is achieved by having a high concentration of solids in the cell and pumping aerated slurry upwards through the cell. The air then has to force its way through the particles, creating the environment for contacting. Experiments have shown improved flotation of coarse galena with particle sizes of up to 850 μm using such a device.

2.2 Turbulence Fundamentals

Flotation is directly influenced by the turbulent environment in which it occurs. It is therefore important to understand turbulence in order to appreciate how it may effect the process of flotation. Turbulence in itself is a complex topic and only a brief overview is given here. This section is derived largely from the review in Nguyen and Schulze (2004).

2.2.1 Turbulent Flow

The instantaneous fluid velocity at a point in a turbulent environment is composed of two parts. These are the mean velocity of the bulk fluid flowing in the system at that point, and a fluctuating component known as the instantaneous fluctuating velocity (u). This fluctuating velocity is the action of turbulent eddies in the system, and it is this velocity which is thought to be of importance in flotation. The root mean squared (RMS) fluctuating velocity can be defined as $u' = \sqrt{\overline{u}^2}$ in each direction. If the velocity is denoted u, v and w in the x, y and z direction respectively, then the total kinetic energy (TKE) can be described as:

$$TKE = \frac{1}{2}(u'^2 + v'^2 + w'^2) \tag{2.1}$$

If the turbulence is assumed to be isotropic, then the RMS turbulent velocities are equal in all directions. Therefore u'=v'=w' and Equation 2.1 becomes:

$$TKE = \frac{3}{2}(u'^2) \tag{2.2}$$

This assumption of isotropy is made for most collision models for flotation, however it is not strictly true in most flotation devices. The rate of turbulent energy dissipation (ϵ) can be defined as:

$$\epsilon = -\frac{dTKE}{dt} \tag{2.3}$$

In flotation literature and practice the average energy dissipation ($\overline{\epsilon}$) is commonly used, which can be determined from the power input into the system (P) and the mass of the fluid being agitated (m_L).

$$\overline{\epsilon} = \frac{P}{m_L} \tag{2.4}$$

This assumes that the energy dissipation is homogeneous in the cell which is generally not the case, however it serves as measure of the overall energy dissipation in a flotation cell.

2.2.2 The Turbulent Energy Spectrum

The eddies in a turbulent system are described as a spectrum of different sizes (λ) through which the energy cascades. The total kinetic energy as described in Section 2.2.1 is due to the action of all the eddies in the spectrum. Energy is continuously transferred, through turbulent shear stress, from large eddies to successively smaller eddies until the smallest possible eddies are reached, which then dissipate the energy as heat. A schematic of the turbulent energy spectrum is shown in Figure 2.4.

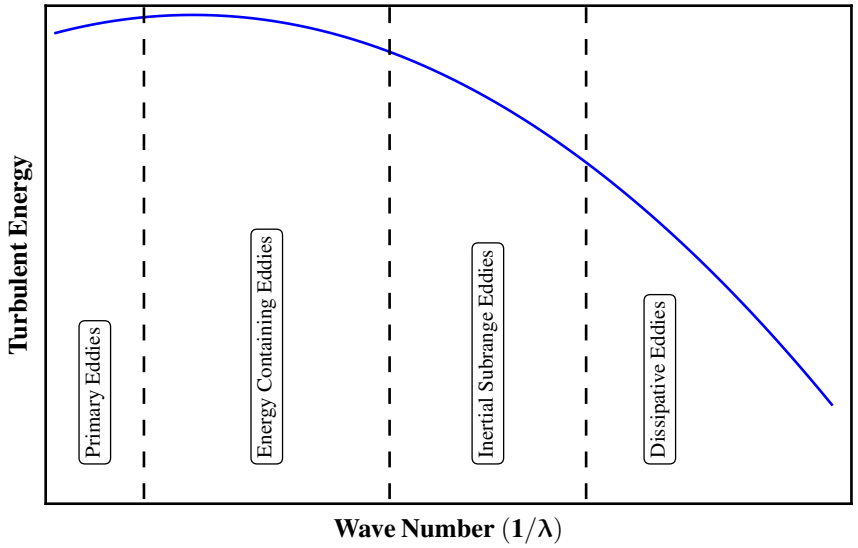

Figure 2.4: Schematic of the turbulent energy spectrum.

Energy is initially input into a system through some external means (for example an impeller or an oscillating grid) to form primary eddies. The energy is transferred to smaller eddies which contain the majority of the energy in the system and are known as the energy containing eddies. As the eddy size decreases the number of eddies increases, but the total energy contained in that eddy size decreases. Eddies smaller than the energy containing eddies are known as the inertial subrange eddies, as inertial forces are dominant in them. The smallest eddies in the spectrum dissipate the energy as heat through molecular friction and are known as the dissipative eddies.

2.2.3 Macro and Micro Scales of Turbulence

The eddies in the turbulent energy spectrum have defined scales which can be quantified. The large scale primary and energy containing eddies are thought to have a size (Λ) which is in the order of magnitude of the turbulence generating device (for example the impeller), and are known as the macroscale of turbulence. Smaller scale eddies in the inertial and dissipative subrange are thought to be independent of the external means of energy input, and the turbulence is often referred to as microturbulence. Kolmogorov (1941) proposed that these smallest eddies are dependent entirely

on the energy dissipation rate (ϵ) and the kinematic viscosity of the fluid (ν). The smallest possible eddies are known as the Kolmogorov microscale, and have a length (η) and velocity (ω) defined as:

$$\eta = \left(\frac{\nu^3}{\epsilon}\right)^{\frac{1}{4}} \tag{2.5}$$

$$\omega = (\nu\epsilon)^{\frac{1}{4}} \tag{2.6}$$

where ν is the kinematic viscosity of the fluid and ϵ is the energy dissipation. Microturbulence can be separated into the inertial and dissipative subranges. Eddies that have radii $r < (5 \text{ to } 10)\eta$ are considered to be in the dissipative subrange and are laminar. Eddies with radii $0.06\Lambda > r > (15 \text{ to } 20)\eta$ are considered to be in the inertial subrange and are turbulent within themselves. The scale of the largest laminar eddies and smallest turbulent eddies, at typical flotation energy dissipations, are given in Table 2.1.

Table 2.1: Scales of microturbulence relevant to flotation.

Dissipation Rate (kW/m^3)	**Largest Laminar eddies (μm)**	**Smallest Turbulent eddies (μm)**
1	160 – 320	470 – 630
3	120 – 240	360 – 480
5	105 – 210	310 – 420

From Table 2.1 it can be seen that, in a typical flotation environment, particles smaller than 100 μm would be contained within laminar eddies. However, bubbles would typically be approximately 1 mm in size, and would therefore be influenced mainly by the turbulent eddies in the inertial subrange.

2.3 Oscillating Grids

Oscillating grids produce turbulence which, at a distance away from the grid, is considered to be laterally homogeneous and isotropic. In addition to this they have zero-

mean-flow and the energy dissipation can be easily varied. These properties make oscillating grids useful tools for investigating areas which operate in turbulent regimes. Examples of research areas which use oscillating grids are combustion (De-Silva and Fernando, 1994), re-suspension (Orlins and Gulliver, 2003), sedimentation (Huppert et al., 1995), mixing across density layers (McDougall, 1979), coagulation (Brunk et al., 1998), precipitation (Mokgethi, 2010) and flotation (Changunda et al., 2008). This section will describe the hydrodynamics of oscillating grids, and the determination of energy dissipation.

2.3.1 Oscillating Grid Turbulence

Oscillating grid turbulence is generated by moving either a single grid or multiple grids at a stroke length (S) and frequency (f) in a fluid. The movement of the grid openings through the fluid generates jets and wakes which interact, and create turbulence (Yan et al., 2007). Typical oscillating grid set-ups are illustrated in Figure 2.5, which shows both a single and double grid set-up.

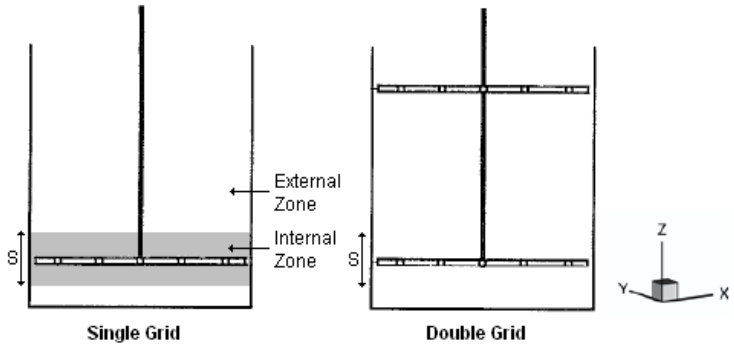

Figure 2.5: Diagram of single and double oscillating grids (adapted from Villermaux et al., 1995).

The turbulence in the system occurs in two distinct areas, namely the area swept by the grid known as the internal region, and the area which is not swept by the grid known as the external region. The turbulence generated by the grids is directional and, for the purposes of this review, the horizontal plane is taken to be the x and y directions whilst the vertical (direction of oscillation) is the z direction.

2.3.1.1 Single Grids

The majority of studies into oscillating grid turbulence have been conducted using single oscillating grids (Hopfinger and Toly, 1976; McDougall, 1979; De-Silva and Fernando, 1994; Huppert et al., 1995; Liem et al., 1999; Orlins and Gulliver, 2003) and are reviewed briefly here. Hopfinger and Toly (1976) gave the following relationship describing the RMS fluid velocities in the external region generated by a single oscillating grid:

$$\begin{aligned} u^{'} = v^{'} = C_1 M^{0.5} S^{1.5} f h^{-1} \quad & \text{Horizontal (x,y) plane} \\ w^{'} = C_2 M^{0.5} S^{1.5} f h^{-1} \quad & \text{Vertical (z) plane} \end{aligned} \tag{2.7}$$

where h is the distance in the z axis away from the grid, M is the spacing of the mesh in the grid, and C_1 and C_2 are constants given as 0.25 and 0.27 respectively. The RMS velocities in the x and y directions ($u^{'}$ and $v^{'}$) are equal, but the RMS velocity in the z direction is slightly larger. It is due to this, that this type of turbulence is considered to be nearly isotropic. The measured TKE around a single oscillating grid (Orlins and Gulliver, 2003) is depicted in Figure 2.6.

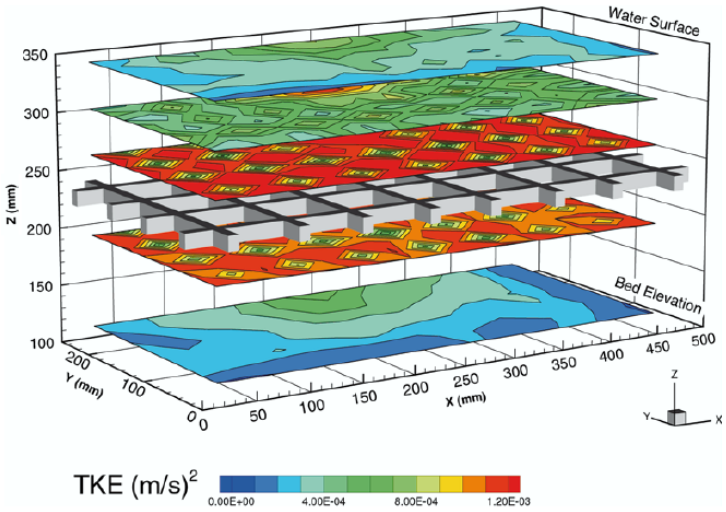

Figure 2.6: Distribution of TKE generated by a single oscillating grid operating at 5 Hz and 30 mm (from Orlins and Gulliver, 2003).

It is illustrated in Figure 2.6 that the turbulence is laterally homogeneous and decreases away from the grid, as indicated by Equation 2.7. The TKE is higher at the areas opposite the nodes of the grid, this is a characteristic of oscillating grids which is considered to be unavoidable. Shy et al. (1997) found that this difference between node and hole decreases as one measures further away from the grid.

Equation 2.7 is only applicable for turbulence in the external region and does not describe the turbulence in the internal region. Bache and Rasool (1996) studied the turbulence in the internal zone of a single grid system. It was found that the areas swept by the grid have significantly higher RMS velocities and energy dissipation levels than in the remainder of the cell. Brunk et al. (1998) measured the turbulence parameters in the internal region in a single grid system. It was found that the TKE in the internal region did not vary greatly with distance from the center of oscillation.

2.3.1.2 Multiple Grids

It has been shown in Equation 2.7 and Figure 2.6 that the turbulence in a single oscillating grid system degrades with distance from the grid. In order to remedy this researchers have used two grids which generate a stationary zone of interest between them (Villermaux et al., 1995; Srdic et al., 1996; Shy et al., 1997). Villermaux et al. (1995) proposed that the RMS velocities are additive when considering multiple grids, and the effective turbulent RMS velocity (u'_{eff}) can be given as:

$$u'_{eff} = 2^{\frac{1}{3}} u' \tag{2.8}$$

This equation was experimentally validated by Shy et al. (1997), who also determined that the area between the grids was nearly isotropic and stationary. Bache and Rasool (2001) investigated the turbulence in a multiple grid cell consisting of 19 grids. In accordance with other researchers, it was found that eddy motion was higher in the z direction. In the areas swept by the grid it was found that $w'^2 \approx 4u'^2$, and due to this an average intensity per direction (U'^2) was defined in order to account for this anisotropy in the system.

$$U'^2 = \frac{1}{3}(2u'^2 + w'^2) \tag{2.9}$$

The measured value of U'^2 for the length of the oscillating grid cell, from Bache and Rasool (2001), is shown in Figure 2.7.

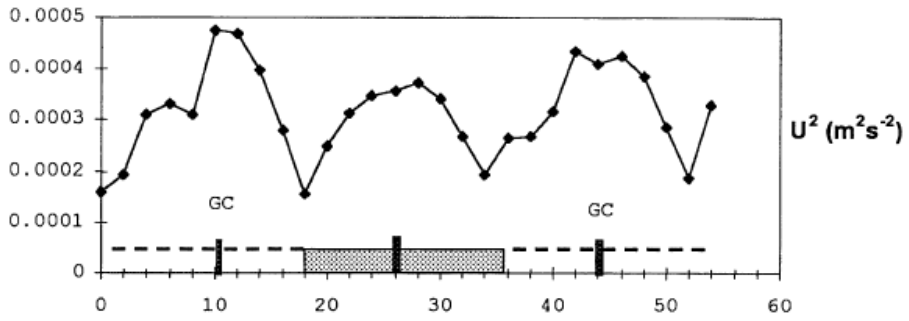

Figure 2.7: Graph showing U'^2 variation with tank height, at 2 Hz and 18 mm amplitude. (from Bache and Rasool, 2001).

It can be seen in Figure 2.7 that U'^2 was relatively constant throughout the cell. Note that in Figure 2.7 the stroke length is equal to the spacing between the grids and therefore the entire length is swept by the grids. It is assumed that for a multi-grid scenario, under these conditions, the turbulence can be considered homogeneous through out the cell.

2.3.1.3 Deviations from Ideal Hydrodynamic Behaviour

There is evidence that, at high frequencies, oscillating grid turbulence deviates from being isotropic. It has been suggested by McDougall (1979) that 7 Hz should be the highest frequency used (known as the "off" frequency) since after this point u', v' and w' no longer increase linearly with frequency, and therefore Equation 2.7 no longer holds. Shy et al. (1997) found that in the case of a double grid system this effect began at approximately 9 Hz. These observations are however made in the external region only and it is not known how higher frequencies may effect the internal region.

There have been reports of undesired circulatory flows in single grid cells (McDougall, 1979; McKenna and McGillis, 2004). It was found that these flows were dependent on initial starting conditions and McDougall (1979) noted that they began when seeding material was added. McKenna and McGillis (2004) concluded that circulatory flows are a feature of oscillating grid turbulence, but they are relatively benign if sufficiently

spaced sampling points are used. These observations have only been made in single grid systems and it is not known if they may be a feature in multiple grid systems.

Villermaux et al. (1995) conducted experiments on a double grid system to observe intense vortical structures using a migrating bubble technique. This technique used 100 μm bubbles in water heated to 70°C - 75°C so as to decrease the viscosity. The bubbles then migrate towards areas of low pressure, in this case the vortical structures. It was observed that the structures were short lived and occurred most often near the walls.

2.3.2 Mean Energy Dissipation in Oscillating Grid Agitation

The mean energy dissipation is a parameter which is often used in flotation literature and practice. In this section the determination of energy dissipation in an oscillating grid cell is discussed. The review presented here is derived from the work of Bache and Rasool (1996) and Guadayol et al. (2009). In an oscillating grid cell the energy dissipation originates from the oscillating motion of the grids through the fluid. This motion of the grid stack can be described, in terms of displacement (Y), velocity ($\dot{Y}$) and acceleration ($\ddot{Y}$), as follows:

$$\begin{aligned} Y(t) &= -\frac{S}{2}cos(2\pi ft) \\ \dot{Y}(t) &= S\pi f sin(2\pi ft) \\ \ddot{Y}(t) &= 2S\pi^2 f^2 cos(2\pi ft) \end{aligned} \tag{2.10}$$

As the grid moves through and fluid it exerts a force due to the frictional drag of the plate (Guadayol et al., 2009), this frictional force transfers energy from the grids to the fluid. The frictional force is described by the classical drag force equation:

$$F(t) = \frac{1}{2}C_d\rho_f S_A\dot{Y}(t) \tag{2.11}$$

where C_d is the drag coefficient, ρ_f is the density of the fluid and S_A is the solids area of the grid. The drag coefficient (C_d) is assumed to be constant with time, making

this a quasi-steady state assumption. The instantaneous power input into a system can then be given as:

$$P(t) = F(t)\dot{Y}(t) \tag{2.12}$$

The net power input is given as the integral of power with time over a single oscillation:

$$\overline{P} = \frac{1}{\tau}\int_0^\tau P(t)dt = \frac{1}{\tau}\int_0^\tau F(t)\dot{Y}(t)dt \tag{2.13}$$

where τ is the period of one oscillation and is equal to f^{-1}. Substitution of Equation 2.11 into Equation 2.13 and integration yields (Guadayol et al., 2009):

$$\overline{P} = \frac{2}{3}C_d\rho_f\pi^2 S_A f^3 S^3 \tag{2.14}$$

The mean energy dissipation can be calculated by:

$$\overline{\epsilon} = \frac{\overline{P}}{m_L} \tag{2.15}$$

where m_L is the mass of fluid being agitated. If it is assumed that energy dissipation is additive for multiple grids, then for a system with n grids the average energy dissipation can be described by:

$$\overline{\epsilon} = \frac{n\frac{2}{3}C_d\rho_f\pi^2 S_A f^3 S^3}{m_L} \tag{2.16}$$

Energy dissipation is therefore strongly dependent on the frequency and stroke of oscillation and these are the key operating variables in an oscillating grid system.

2.4 Effect of Energy Dissipation on Flotation Kinetics: Theoretical Findings

In this section the theoretical models of flotation in a turbulent environment will be discussed. Flotation is most commonly described by a first order reaction with the form:

$$\frac{dN_p}{dt} = -kN_p \tag{2.17}$$

where k is the flotation rate constant and N_p is the number of particles per unit volume. Flotation modelling generally aims to derive models for the flotation rate constant. In a quiescent system the rate constant can be calculated from (Jameson et al., 1977):

$$k = \frac{3QE_{coll}H}{2d_bV_c} \tag{2.18}$$

where Q is the gas volumetric flowrate, H is the height of the cell, V_c is the cell volume and E_{coll} is the collection efficiency, which can be defined as the fraction of particles in the path of a bubble, that successfully attach to the bubble and rise to the froth (Jameson et al., 1977). Equation 2.18 does not take energy dissipation into account and therefore studies have been conducted to model flotation in turbulent systems. For flotation in turbulent systems the rate equation can be written as (Julien Saint Amand, 1999; Koh and Schwarz, 2003; Pyke, 2004; Sherrell, 2004; Newell and Grano, 2006):

$$\frac{dN_p}{dt} = -kN_p = -Z_{pb}E_{coll} \tag{2.19}$$

where Z_{pb} is the rate or frequency of particle-bubble collisions per unit volume and is dependent on the energy dissipation in the system. The flotation rate constant (k) can then be defined as:

$$k = \frac{Z_{pb}E_{coll}}{N_p} \tag{2.20}$$

The elements which make up the collection efficiency are discussed in Section 2.4.1, and the frequency of particle-bubble collisions is discussed in Section 2.4.2. The

findings of studies which have derived and used general flotation models are reviewed in Section 2.4.3.

2.4.1 Particle - Bubble Collection Efficiency

The collection efficiency is considered to be comprised of three sub-processes which describe the ability of a particle to be floated, and are discussed separately in this section. These sub-processes are the collision of a particle with a bubble, the attachment of a particle to a bubble and detachment of a particle from a bubble. The collection efficiency can then be expressed as:

$$E_{coll} = E_c E_a E_s \tag{2.21}$$

where E_c is the collision efficiency, E_a is the attachment efficiency and E_s is the stability efficiency. The majority of the concepts stem from work done by Sutherland (1948) with a large body of work dedicated to it since then. This work has been thoroughly reviewed by many authors (Deglon, 1998; Ralston et al., 1999; Pyke, 2004; Sherrell, 2004; Anderson, 2008; Miettinen et al., 2010) and this review is derived from those works.

2.4.1.1 Particle - Bubble Collision Efficiency

When a particle and bubble approach one another in a fluid they may not necessarily collide, but the particle may rather move with the fluid streamlines around the bubble. The collision efficiency is therefore dependent on the streamlines around a bubble, and the tendency of the particles to stay in the streamlines. The particle trajectory in the fluid flow and its tendency to stay in the streamlines can be characterised by the Stokes number:

$$St = \frac{\rho_p v_b d_p^2}{9 d_b \mu_f} \tag{2.22}$$

where d_b and v_b are the bubble diameter and rise velocity, ρ_p and d_p are the particle density and diameter and μ_f is the fluid viscosity. When $St << 1$ the particles are

considered to have negligible inertia and will follow the fluid streamlines. When St $>>$ 1 the particles will be relatively unaffected by the fluid streamlines. The flow of fluid around a bubble can be described by the bubble Reynolds number.

$$Re_b = \frac{v_b \rho_f d_b}{\mu_f} \tag{2.23}$$

For $Re_b << 1$ the flow is considered to be in the Stokes regime, and potential flow when $80 < Re_b < 500$. Flow conditions which fall between the Stokes and potential flow regimes are known as the intermediate flow regime.

Various models for the efficiency of collision have been derived for the different flow regimes. For potential flow ($80 < Re_b < 500$), negligible particle inertia (particles follow that streamlines) and an immobile bubble surface the following model derived by Sutherland (1948) holds.

$$E_{c,S} = 3\frac{d_p}{d_b} \tag{2.24}$$

Gaudin (1957) derived a model describing collision in the Stokes flow regime ($Re_b << 1$), neglecting particle inertia and assuming an immobile bubble surface.

$$E_{c,G} = \frac{3}{2}\left(\frac{d_p}{d_b}\right)^2 \tag{2.25}$$

Yoon and Luttrell (1989) derived a model for the intermediate flow regime, that assumed negligible particle inertia and an immobile bubble surface.

$$E_{c,Y} = \left(\frac{3}{2} + \frac{4Re_b^{0.72}}{15}\right)\left(\frac{d_p}{d_b}\right)^2 \tag{2.26}$$

This model has been used in various studies for flotation modelling (Koh and Schwarz, 2006; Evans et al., 2008; Jameson, 2010). Equations 2.24 – 2.26 are limited by the fact that they do not account for particle inertia or mobile bubble surfaces. Dai et al.

(1998) derived a model for collision efficiency in the potential flow regime which accounts for both particle inertia and mobile bubble surface:

$$E_{c,GSE} = E_{c,S}\sin^2\theta_t \exp\left[3K_3\cos\theta_t\left(\ln\frac{3}{E_{c,S}} - 1.8\right) - \frac{9K_3\left(\frac{2}{3} + \cos^3\theta_t - \cos\theta_t\right)}{2E_{c,S}\sin^2\theta_t}\right] \tag{2.27}$$

where $E_{c,S}$ is the Sutherland (1948) model as given in Equation 2.24. θ_t is the angle of tangency or maximum collision angle, given as:

$$\theta_t = \arcsin\left[2\beta\left(\sqrt{1+\beta^2} - \beta\right)\right]^{\frac{1}{2}} \tag{2.28}$$

where K_3 and β are dimensionless numbers given by:

$$K_3 = \frac{2v_b(\rho_p - \rho_f)r_p^2}{9\mu r_b} \tag{2.29}$$

$$\beta = \frac{4E_{c,S}}{9K_3} \tag{2.30}$$

This equation is known as the Generalised Sutherland Equation (GSE) and has been used in a number of flotation models (Pyke, 2004; Sherrell, 2004; Newell and Grano, 2006). The model predicts increased collision efficiency with increasing particle size and decreasing bubble size. Dai et al. (1998) showed that Equation 2.27 was in agreement with experimental data from quartz flotation with particle sizes of 7 – 60 μm and Stokes numbers of up to 0.27. Collision efficiencies were found to be in the range of 0.01 – 0.1 which is considerably smaller than the theoretical maximum of 1, emphasising the low collision efficiencies for fine particles.

2.4.1.2 Particle - Bubble Attachment Efficiency

Once a particle and a bubble have successfully collided the particle must become attached to the bubble for flotation to proceed. The success of attachment depends largely on the hydrophobicity of the particle and is therefore the primary selective

process in flotation. In order to model attachment two critical factors are considered, sliding time and induction time. If we consider a particle colliding with a bubble, the particle will make contact with the bubble and then slide around the circumference to a point, beyond which it will move away from the bubble. Sliding time is thus the time that a particle spends touching, or sliding along a bubble. Induction time is the time required for the particle to become attached to the bubble. If the sliding time is greater than the induction time then the particle can become attached to the bubble (Sutherland, 1948).

Dobby and Finch (1986) proposed a model based on two collision angles between a particle and bubble, measured from the vertical. The first is the adhesion angle (θ_a), which is the angle at which the sliding time will equal the induction time and the particle will attach. The second is the maximum possible collision angle, or angle of tangency (θ_t). The attachment efficiency is then described by:

$$E_a = \frac{\sin^2\theta_a}{\sin^2\theta_t} \tag{2.31}$$

The adhesion angle (θ_a) can be calculated from (Dobby and Finch, 1986):

$$\theta_a = 2\arctan\exp\left[-t_{ind}\frac{2(v_p+v_b)+v_b\left(\frac{d_b}{d_p+d_b}\right)^3}{d_p+d_b}\right] \tag{2.32}$$

where v_p and v_b are the velocities of the particle and bubble respectively, and t_{ind} is the induction time, which can be calculated by the empirical equation (Dai et al., 1999):

$$t_{ind} = Ad_p^B \tag{2.33}$$

where B is a constant and A is inversely proportional to the contact angle of the particle. A and B are both determined from experimental data. The angle of tangency (θ_t) was given by Dobby and Finch (1986) as a set of equations, derived from experimental data, which are not reproduced here. Dai et al. (1999) proposed that Equation 2.28 from the GSE equation for collision may be used to calculate θ_t. In this case the model is known as the modified Dobby and Finch model and has been used by Pyke (2004) and Newell and Grano (2006) in general flotation models.

This model predicts that attachment efficiency increases with decreasing particle size, decreasing bubble size and increasing contact angle. Dai et al. (1998) showed that the model was in agreement with experimental data from the flotation of quartz with particle sizes of 7.5 – 70 μm and contact angles between 33° and 74°.

Yoon and Mao (1996) proposed a model based on the the extended DLVO theory which includes surface properties of the particles and bubbles. This method focuses on the interaction of different forces and energies in the system. The attachment efficiency in this case is given as:

$$E_a = \exp\left(-\frac{E_1}{E_{k-A}}\right) \tag{2.34}$$

where E_1 is the maximum energy that must be overcome in order for attachment to occur, and requires experimental data to calculate (Yoon and Mao, 1996). $E_{k\text{-}A}$ is the kinetic energy available in the system to overcome the energy barrier of attachment. Sherrell (2004) proposed that in turbulent systems the energy available to the particles/bubbles is the total turbulent kinetic energy ($TKE_{k\text{-}A}$) of the turbulent eddies which are of the same size, or smaller than the particles/bubbles. It is therefore taken to be the average energy between the eddies of the same scale of the particles/bubbles and the smallest possible eddies (Kolmogorov microscale). The energy available for attachment is given as:

$$E_{K-A} = \frac{1}{2}(m_p + m_b)TKE_{k-A} \tag{2.35}$$

where m_p and m_b are the mass of the particle and bubble respectively. Since all the energy available to the turbulent eddies originates from external agitation (the impeller in a stirred cell), the attachment efficiency is linked to the energy dissipation in the system and would be expected to increase with increasing energy dissipation.

This model only takes thermodynamics effects into account and neglects the physical aspects. It can be shown (Pyke, 2004) that the equation contradicts theoretical and experimental data by predicting an increased attachment efficiency with increased particle size. Despite this, the model has been used in flotation modelling (Sherrell, 2004).

2.4.1.3 Particle - Bubble Stability Efficiency

Once a particle and bubble are attached they may break apart again, this is known as detachment and depends on the stability of the particle-bubble aggregate. The stability efficiency can be described by the theory proposed by Schulze (1977, 1982) and is therefore often referred to as the Schulze model. The description presented here follows the review in Nguyen and Schulze (2004). The stability of a particle-bubble aggregate is described by the combination of all the forces acting to detach the particle from the bubble (f_{det}) and the tenacity of the particle attachment (T). The stability efficiency is then described by the exponential relationship (Nguyen and Schulze, 2004):

$$E_s = 1 - \exp\left(1 - \frac{T}{F_{det}}\right) \tag{2.36}$$

The tenacity of particle attachment stems from the hydrophobicity of the particle and is given by:

$$T = 0.5\pi d_p \sigma (1 - cos\theta) \tag{2.37}$$

where σ is the surface tension and θ is the contact angle. The detachment force in a turbulent environment can be considered to occur due to accelerative forces on the aggregate and is given as:

$$F_{det} = \frac{\pi d_p^3 (a + g)\Delta\rho}{6} \tag{2.38}$$

where a is the acceleration of the aggregate due to the turbulence, g is the acceleration due to gravity and $\Delta\rho$ is the difference between the fluid density and particle density. The acceleration of the aggregate (a) due the movement of the fluid is calculated assuming that the aggregates have a centrifugal acceleration equivalent to the

centrifugal acceleration of the turbulent eddies of similar size to the aggregate. In the inertial subrange of turbulence this is given as:

$$a = 1.9\frac{\overline{\epsilon}^{\frac{2}{3}}}{\left(\frac{d_p}{2}+\frac{d_b}{2}\right)^{\frac{1}{3}}} \tag{2.39}$$

And for the viscous dissipation subrange:

$$a = 0.52\frac{\overline{\epsilon}^{\frac{3}{4}}}{\nu^{\frac{1}{4}}} \tag{2.40}$$

In a typical flotation application the aggregate will likely be in the inertial subrange (see Table 2.1) and therefore Equation 2.39 will be applicable. Substitution of the the tenacity (Equation 2.37) and the detachment forces (Equation 2.38) into Equation 2.36 gives the relationship:

$$E_s = 1 - \exp\left(1 - \frac{3\sigma(1-cos\theta)}{d_p^2(a+g)\Delta\rho}\right) \tag{2.41}$$

This model predicts increasing detachment with increasing particle size, increasing energy dissipation, decreasing particle contact angle (hydrophobicity) and decreasing aggregate size.

Another approach is to consider the energies associated with the aggregate. Sherrell (2004) used a Arrhenius type equation to describe the stability efficiency:

$$E_s = 1 - \exp\left(-\frac{W_A}{E_{k-D}}\right) \tag{2.42}$$

where W_A is the work of adhesion and $E_{k\text{-}D}$ is the kinetic energy of detachment. The work of adhesion (W_A) is the energy required to separate a particle-bubble aggregate and as is given as (Mao and Yoon, 1997):

$$W_A = \frac{1}{4}\sigma\pi d_p^2(1-cos\theta)^2 \tag{2.43}$$

The energy available for detachment was considered to correspond to the kinetic energy of the largest eddies in the system, since all particles are subjected to these eddies and they contain the greatest amounts of energy for detachment. In an impeller agitated system this is considered to be the kinetic energy of the impeller:

$$TKE_{k-D} = (R_{imp}\omega_{imp})^2 \tag{2.44}$$

where R_{imp} is the diameter of the impeller and ω_{imp} is the impeller rotational velocity. The kinetic energy for detachment is then given as:

$$E_{k-D} = \frac{1}{2}(m_p + m_b)TKE_{k-D} \tag{2.45}$$

This model predicts increasing detachment with increasing particle size, increasing energy dissipation and decreasing particle contact angle.

2.4.2 Particle - Bubble Collision Frequency

The rate of collision between particles and bubbles (Z_{pb}) is dependent on the hydrodynamics of the fluid in which they are contained. Different models apply depending on the turbulent regime that the particles and bubbles are contained in. For particles and bubbles which are contained within the smallest turbulent eddies, the collision rate is given as (Saffman and Turner, 1956):

$$Z_{pb} = \sqrt{\frac{8\pi}{15}} N_p N_b \left(\frac{d_p + d_b}{2}\right)^3 \left(\frac{\epsilon}{\nu}\right)^{1/2} \tag{2.46}$$

For Equation 2.46 to hold, the particles and bubbles must be small compared to the smallest eddies in the fluid. It is therefore only applicable to low energy dissipation and is generally not suitable for normal flotation systems. For example, consider a system with an average energy dissipation of 1 kW/m^3, which is relatively low for flotation, the smallest laminar eddy is approximately 130 μm (Schubert, 1999). In a typical flotation operation the fine particles would fall in this range, however the bubbles would be well above this size. This equation has been used to model the

collision rates in the low dissipation regions of flotation cells (away from the impeller) in CFD modelling of flotation (Koh and Schwarz, 2003, 2006; Evans et al., 2008).

Abrahamson (1975) proposed the following equation for collision in highly turbulent fluids, where particles are randomly flung between turbulent eddies:

$$Z_{pb} = 5N_pN_b\left(\frac{d_p + d_b}{2}\right)^2\sqrt{u_p^{'2} + u_b^{'2}} \tag{2.47}$$

where $u_p^{'}$ and $u_b^{'}$ are the RMS relative velocity for the particles and bubbles respectively. It is assumed that the colliding particles' velocities are independent, in magnitude and direction. For this assumption to hold the following condition must be met (Abrahamson, 1975):

$$d_{p/b}^2 > \frac{15\mu_f u_f^{'2}}{\rho_{p/b}\epsilon} \tag{2.48}$$

It can be shown (Anderson, 2008) that this condition is not met in typical flotation cells. This model has however been used in many flotation studies in turbulent systems (Jordan and Spears, 1990; Schubert, 1999; Duan et al., 2003; Pyke et al., 2003; Sherrell, 2004; Koh and Schwarz, 2006; Evans et al., 2008). In order to calculate the collision rate from Equation 2.47 the particle and bubble root mean squared velocity ($u_p^{'2}$ and $u_b^{'2}$) are required to be quantified. Various models have been proposed to calculate this. Abrahamson (1975) proposed the following equation:

$$u_{p/b}^{'2} = \frac{u_f^{'2}}{1 + \frac{1.5\tau_{p/b}\epsilon}{u_f^{'2}}} \tag{2.49}$$

where $\tau_{p/b}$ is the relaxation time of a particle/bubble and is a measure of the tendency of a particle or bubble to come to equilibrium in a fluid. Liepe and Mockel (1976) derived an equation empirically using data taken from many other researchers.

$$u_{p/b}^{'} = 0.4\frac{\epsilon^{4/9}d_{p/b}^{7/9}}{\nu^{1/3}}\left(\frac{\rho_{p/b} - \rho_f}{\rho_f}\right)^{2/3} \tag{2.50}$$

Equation 2.50 was derived for particles, although it has been used in the literature for bubbles. Lee and Erickson (1987) derived a model for the RMS bubble fluctuating velocity:

$$u^{'2} = C_0(\epsilon d_b)^{2/3} \tag{2.51}$$

where C_0 is a constant equal to 2 (Batchelor, 1951).

Brady et al. (2006) tested various models for determining the RMS velocity, for both particles and bubbles, in isotropic turbulence formed by fluid flowing through cylindrical grids. It was found that the Liepe and Mockel model predicted the velocity of 80 μm particles reasonably well, while the Abrahamson model was in good agreement with experimental data for 1.2 mm bubbles. The Abrahamson model did, however, also provide reasonable agreement for particles. Both the Liepe and Mockel model, and the Lee and Erickson model over predicted the RMS velocity for bubbles. These results suggest that, when determining the RMS velocity, it may be useful to use the Abrahamson model to model bubble velocities, and the Liepe and Mockel model for particles.

In the flotation literature the Liepe and Mockel (1976) model is most commonly used, for both bubbles and particles (Jordan and Spears, 1990; Julien Saint Amand, 1999; Schubert, 1999; Duan et al., 2003; Pyke et al., 2003; Koh and Schwarz, 2006; Evans et al., 2008). In a standard flotation system $d_b >> d_p$, then $u_p^{'}$ can be neglected, and substituting Equation 2.50 into 2.47 yields (Julien Saint Amand, 1999; Pyke et al., 2003):

$$Z_{pb} = 5N_pN_bd_b^2\left(0.4\frac{\epsilon^{4/9}d_b^{7/9}}{\nu^{1/3}}\right)\left(\frac{\rho_f-\rho_b}{\rho_f}\right)^{2/3} \tag{2.52}$$

If it is assumed that E_{coll} is independent of energy dissipation then the flotation rate constant is proportional to the collision frequency (Equation 2.20). From the two models of collision rates (Equations 2.46 and 2.52) the following relationship between energy dissipation and flotation rate can be shown (Julien Saint Amand, 1999):

$$k \propto Z_{pb} \propto \epsilon^r \quad \text{where} \quad 0.44 < r < 0.5 \tag{2.53}$$

An alternative model was proposed by Nonaka et al. (1982) who assumed that particles and bubbles collide due to turbulent diffusion, and calculated that $k \propto \epsilon^{0.75}$. This relationship was confirmed experimentally for the flotation of quartz in an impeller agitated cell.

Models for describing collision and attachment efficiencies (see Section 2.4.1) are derived for bubbles rising in a stationary fluid, and are dependent on the bubble rise velocity (v_b) which is well defined in quiescent systems. However the use of the bubble rise velocity may not be suitable when modelling flotation in turbulent fluids. Jameson (2010) proposed that in a shearing flow the bubble rise velocity can be replaced with:

$$v_b^{'} = G d_b \tag{2.54}$$

where G is the shear rate, which can be expressed in terms of energy dissipation as (Camp and Stein, 1943):

$$G = \left(\frac{\epsilon}{\nu}\right)^{1/2} \tag{2.55}$$

After substitution into the collection efficiency equation given by Yoon and Luttrell (1989) (Equation 2.26) and using the rate of collision given by Saffman and Turner (1956) (Equation 2.46), it can be shown that $k \propto G^{1.5} \propto \epsilon^{0.75}$ (Jameson, 2010). This is a stronger relationship than other models propose (see Equation 2.53).

2.4.3 General Flotation Models

Theoretical studies have been conducted, which utilise the relevant models describing collection efficiency and particle-bubble collision frequency, to derive general flotation models for turbulent systems. These models take into account such flotation parameters as particle size, bubble size, contact angle/particle hydrophobicity, energy dissipation and gas flowrate. Two general flotation models are briefly reviewed in this section.

Pyke et al. (2003) derived a general flotation model, that was based on the Abrahamson model (Equation 2.47) for collision frequency, and the Liepe and Mockel model

(Equation 2.50) for the bubble RMS velocity. The collision efficiency was described by the generalised Sutherland equation (Equation 2.27), the attachment efficiency by the modified Dobby and Finch model (Equation 2.31), and the stability efficiency by the Schulze model (Equation 2.36). The general flotation model was used to calculate the theoretical flotation rates of sub 80 μm quartz, with moderate to high hydrophobicity, and floated with 0.14 mm bubbles. It was shown that, at low energy dissipations, the flotation rate was essentially described by the collision efficiency, and increased approximately linearly with particle size. Increasing the energy dissipation resulted in increased calculated flotation rates, due to increased particle-bubble collision frequencies. At high energy dissipation the flotation rates for coarse particles decreased, due to low stability efficiencies. The model predictions were compared with experimental data from batch floats of quartz with a particle size of 8 – 80 μm. The results showed good agreement between the experimental and calculated flotation rates, when the values for the bubble velocity and energy dissipation used in the calculation corresponded to those measured away from the impeller zone of the flotation cell.

Newell and Grano (2006) fitted the model derived by Pyke et al. (2003) to experimental data from quartz floats, in different sized batch cells, operating at various energy dissipations. It was found that using the measured bubble rise velocity in the model calculations resulted in the model underestimating the experimental flotation rates. The model was therefore fitted to the experimental data using the bubble velocity as a variable.

A general flotation model was derived by Sherrell (2004), using the generalised Sutherland equation (Equation 2.27) for collision efficiency, and the energy based models for the attachment and stability efficiencies (Equations 2.34 and 2.42). The Abrahamson model (Equation 2.47) was used for collision rates, along with the Liepe and Mockel model (Equation 2.50) for particle RMS velocity, and the Lee and Erickson model (Equation 2.51) for bubble RMS velocity. It was found that the model predictions showed reasonable agreement with experimental data from the flotation of glass beads with varied contact angles, percent solids and energy dissipations. The greatest discrepancies between the experimental and theoretical flotation rate constants occurred when the flotation experiments were conducted at a high percent solids, using large particles with low contact angles.

2.5 Effect of Energy Dissipation on Flotation Kinetics: Experimental Findings

In this section the findings from experimental studies on flotation kinetics are reviewed. This review is limited to those studies which investigated the effects of particle size, bubble size and energy dissipation on single mineral flotation rates, since these are relevant to this investigation.

2.5.1 The Effect of Particle Size on Flotation Kinetics

The relationship between particle size and flotation rate is well established in flotation literature. Fine particles float slowly due to poor collision with bubbles, as they tend to move in the fluid streamlines around the bubbles (Sutherland, 1948). Coarse particles also float poorly as they are more susceptible to detachment. There is therefore an optimum particle size for flotation. The general form of the relationship between particle size and flotation rate for fine particles (below the optimum size for flotation) can be described by the power equation $k \propto d_p^n$.

Jameson et al. (1977) reviewed various literature studies (Reay and Ratcliff, 1975; Collins and Jameson, 1976; Anfruns and Kitchener, 1977) on the effect of particle size on flotation rates in quiescent systems. It was concluded that, for fine particles (4 $\mu m < d_p < 30$ μm) floated with sub 100 μm bubbles, the value of n was 1.5. Crawford and Ralston (1988) used methylation techniques to render quartz particles hydrophobic to various contact angles. A linear relationship between flotation rate and particle size was found, for particles with contact angles from 50^o to 88^o.

In an agitated cell, Gaudin et al. (1942) found that, for the flotation of galena with particle sizes above 4 μm, the value of n was 1. For particles below 4 μm, the flotation rate was independent of particle size. Trahar (1981) investigated the batch flotation of several sulphide minerals, and found a roughly linear relationship between the flotation rate and particle size, for sub 20 μm particles floated with excess collector. Ahmed and Jameson (1985) floated latex, quartz and zircon in a stirred cell, and found that there is a weaker relationship between particle size and the flotation rate than Jameson et al. (1977) suggests, with $n < 1$ for the flotation of quartz and zircon.

Deglon (1998) found n to be 0.15 and 0.38, for the flotation of sub 32 μm and sub 100 μm quartz respectively. Pyke et al. (2003) found that, for quartz flotation at low energy dissipations, the relationship is approximately linear. Changunda et al. (2008) floated sub 100 μm quartz in an oscillating grid cell, using discrete bubble sizes of 0.13 mm, 0.24 mm and 0.82 mm. At an energy dissipation of 0.44 kW/m^3 it was found that $k \propto d_p^1$ for all bubble sizes used.

2.5.2 The Effect of Bubble Size on Flotation Kinetics

It is well established in the flotation literature that flotation rates increase with decreasing bubble size. This effect is due to the increased number of bubbles when using smaller bubbles, as well as the increased collision efficiency of small bubbles (Jameson et al., 1977). The relationship between flotation rate and bubble size is commonly expressed as the inverse power equation $k \propto d_b^{-m}$.

Jameson et al. (1977) reviewed the literature (Reay and Ratcliff, 1975; Collins and Jameson, 1976; Anfruns and Kitchener, 1977) and found a value for m of 3, for flotation in quiescent systems with sub 100 μm bubbles. Yoon and Luttrell (1986) found the value of m to be 2.1 – 2.3, for fine coal flotation. Diaz-Penafiel and Dobby (1994) found the value for m to be 1.15 – 2.08, for the flotation of silica in a column.

Ahmed and Jameson (1985) determined that in a stirred cell the relationship between flotation rate and bubble size is never as strong as in quiescent systems. Deglon (1998) floated sub 32 μm quartz particles in a stirred cell, and found a value for m of 2.2, at low agitation rates. In de-inking flotation, Julien Saint Amand (1999) observed a value for m of 1.5, for the flotation of sub 50 μm ink particles. Changunda et al. (2008) floated sub 100 μm quartz in an oscillating grid cell and found a value of 0.75 for m, at an energy dissipation of 0.44 kW/m^3.

2.5.3 The Effect of Energy Dissipation on Flotation Kinetics

Many experimental studies have been performed in order to gain knowledge on the effect of energy dissipation on flotation. A selection of these studies which used particle sizes of sub 100 μm and bubble sizes of less than 1.2 mm are summarised in

Table 2.2. In these studies the bubble size is controlled independently of the energy dissipation, so as to decouple the effect of energy dissipation and bubble size. The majority of these studies have been conducted in stirred cells, with some work done in an oscillatory baffled column (OBC) and an oscillating grid cell (OGC), which are discussed separately.

Table 2.2: Table of summarised experimental studies on the effect of energy dissipation on flotation kinetics (adapted from Anderson, 2008).

Author	**Ore**	**Agitation**	**Hydrophobicity**	**Energy Dissipation (kW/m^3)**	**Particle Size (μm)**
Ahmed and Jameson (1985)	Quartz Zircon Latex	Stirred Cell	Moderate collector dosage	0.01 - 2.5*	<50
Deglon (1998)	Quartz	Stirred Cell	Low collector dosage	0.1 - 1.9	<32; <100
Pyke (2004)	Quartz Chalcopy-rite Galena	Stirred Cell	Contact angle of 53°-80°	0.45 - 1.8	<75
Newell and Grano (2006)	Quartz	Stirred Cell	Contact angle of 80°	1.25 - 12.6 (0.15 - 1.8)*	<100
Changunda et al. (2008)	Quartz	OGC	Contact angle of 65°	0.015 - 0.6	<100
Anderson (2008)	Quartz	OBC	Low and moderate collector dosage	0 - 0.25	<45

* From Anderson (2008), assuming a power number of 5.5 for a six bladed Rushton turbine.

2.5.3.1 Stirred Cells

Ahmed and Jameson (1985, 1989) were the first to use a system where small bubble generation was decoupled from the impeller speed. This was achieved by sparging a stirred cell with bubbles of a known size. In the study, sub 50 μm latex, zircon and quartz particles were floated using bubble sizes ranging from 0.07 mm to 0.65 mm. From the experiments the effects of bubble size, particle size, particle density

and energy dissipation on flotation kinetics were reported. The effect that particle and bubble size were found to have on flotation kinetics, at low agitation rates, have been discussed in Sections 2.5.1 and 2.5.2.

For the flotation of latex particles, it was found that the flotation rate increased with increased impeller speed, for all particle and bubble sizes used. The dependence of flotation rate on impeller speed was found to be higher when floating with larger bubbles. The results for quartz flotation, using CTAB (2.5 ppm) as the collector, are reproduced in Figure 2.8, for three impeller speeds and three bubble sizes.

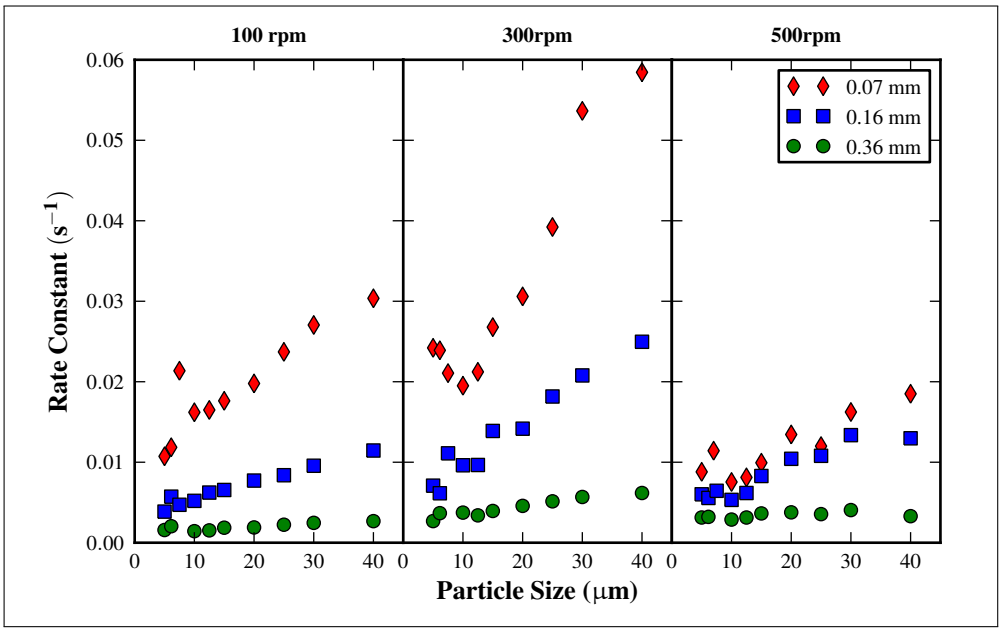

Figure 2.8: Flotation rate constant versus particle size for the flotation of quartz (2.5 ppm CTAB) in a stirred cell, at three agitation rates and bubble sizes (adapted from Ahmed and Jameson, 1985).

Figure 2.8 illustrates that the flotation rate when using sub 0.36 mm bubbles increases with increasing agitation, until a optimum agitation rate (approximately 300 rpm), after which the flotation rate decreases. The rate at which the flotation rate decreases, when the agitation rate is increased from 300 rpm to 500 rpm, increases with decreasing bubble size. Flotation with large bubbles (0.65 mm) resulted in increasing flotation rates with increased agitation, for all agitation rates used (not shown in Figure 2.3). Similar trends were noted for the flotation of zircon. These trends were attributed to increased detachment rates with increased energy dissipation and decreased bubble

size. It was recommended that the optimum conditions for flotation involves small bubbles and the minimum impeller speed required for particle suspension.

Deglon (1998) investigated the effect of energy dissipation on flotation, in a stirred cell similar to that used by Ahmed and Jameson (1985), and sparged with discrete bubble sizes of 0.13 mm, 0.24 mm and 0.82 mm. Quartz (sub 32 μm and sub 100 μm) was floated using HPYC (1.6 x 10^{-5} mol/L) as a collector. The results for the flotation of sub 100 μm quartz, using 0.13 mm and 0.82 mm bubbles, are reproduced in Figure 2.9.

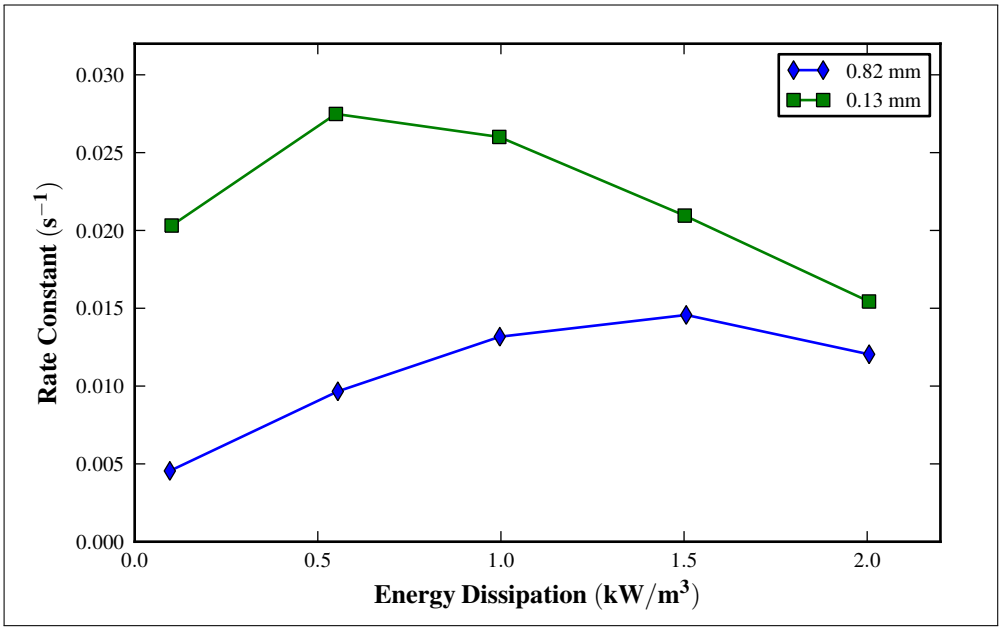

Figure 2.9: Flotation rate constant versus energy dissipation for the flotation of quartz in a stirred cell, for 0.13 mm and 0.82 mm bubbles (adapted from Deglon, 1998).

It is illustrated in Figure 2.9 that the flotation rate increases with increasing energy dissipation to an optimum, after which the flotation rate decreases. These optimum flotation conditions are dependent on the bubble size used, with optimum energy dissipations of 0.65 kW/m^3 and 1.5 kW/m^3 observed, for flotation with 0.13 mm and 0.82 mm bubbles respectively. It is clear from Figure 2.9 that the optimum flotation conditions are small bubbles and low energy dissipations. Further analysis of the data showed that the relationship between flotation rate and energy dissipation followed the form $k \propto \epsilon^{0.91}$ (Deglon, 2002).

Pyke (2004) floated quartz, chalcopyrite and galena in order to investigate the validity of a general flotation model. A stirred cell, similar to that used by Ahmed and Jameson (1985) and sparged with bubbles of approximately 1.2 mm, was used in the study. Quartz (sub 75 μm) was methylated to known advancing contact angles for the flotation experiments. The flotation of quartz, with a contact angle of 73°, resulted in decreasing flotation rates for all particle sizes, when the energy dissipation was increased from 0.45 – 1.45 kW/m^3. The flotation of quartz, with an advancing contact angle of 80°, resulted in flotation rates for fine particles which remained relatively constant, when the energy dissipation was increased from 0.45 – 1.8 kW/m^3. The flotation rates for more coarse particles decreased with increasing energy dissipation over the same range. These results indicated that the effect that energy dissipation has on flotation kinetics was dependent on both the particle size and particle hydrophobicity. Flotation rates decreased, or stayed constant, with increased energy dissipation above 0.45 kW/m^3, this indicates that the optimum energy dissipation for flotation in the system was less than 0.45 kW/m^3. This is low compared to the optimum energy dissipation of 1.5 kW/m^3 found by Deglon (1998) for similar conditions.

Chalcopyrite (density of 4100 kg/m^3) was floated using 100 g/t SEX, which produced particle advancing contact angles of 67°. It was found that the flotation rates for sub 75 μm particles increased when the energy dissipation was increased from 0.6 – 1.7 kW/m^3. Galena (density of 7400 kg/m^3) was floated using 10 g/t DBPhos, which resulted in particle advancing contact angles of 72°. It was observed that flotation rates for sub 75 μm particles increased as the energy dissipation was increased from 1.2 – 1.7 kW/m^3, however the magnitude of the increase was significantly smaller for more coarse particles. Subsequent increases in the energy dissipation resulted in decreased flotation rates for all particle sizes. It was concluded that high particle density results in increased detachment rates.

Newell and Grano (2006) measured the flotation rates of methylated quartz particles, in geometrically similar stirred cells with volumes ranging from 2.25 – 50 dm^3, in order to assess scale-up parameters for flotation cells. In the experiments, 0.65 mm bubbles were used to float quartz with an advancing contact angle of 80°. It was found that increasing the energy dissipation led to a linear increase in flotation rate (ie. $k \propto \epsilon^1$), to an optimum at 4.1 kW/m^3. After this optimum the flotation constant was independent of the energy dissipation.

2.5.3.2 Oscillatory Baffled Column

The oscillatory baffled column (OBC) is a novel cell developed by Anderson (2008), who investigated its use both as a research tool and as a potential industrial cell. The oscillatory baffled column is composed of many circular baffles, which are oscillated vertically in a column in order to produce the agitation. A schematic of the apparatus is shown in Figure 2.10.

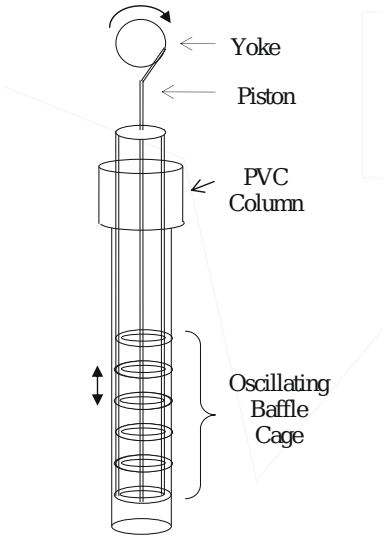

Figure 2.10: Schematic of an oscillatory baffled column (adapted from Anderson, 2008).

In the study, sub 100 μm quartz was floated using a fixed bubble size of 0.6 mm. Energy dissipations of 0.004 – 0.22 kW/m^3 were investigated, these were controlled by changing the oscillating frequency and amplitude of the baffle cage. Particle hydrophobicity was varied by using HPYC (1.6 x 10^{-5} mol/L) and dodecylamine (1 x 10^{-4} mol/L) as collectors, to produce low and moderately hydrophobic particles respectively.

When using low hydrophobicity quartz, the flotation rates for sub 36 μm particles increased with increasing energy dissipation to an optimum at approximately 0.01 kW/m^3. This optimum energy dissipation was an order of magnitude lower than the value of 0.65 kW/m^3 observed by Deglon (1998) in a stirred cell using identical collector surface coverage conditions. The flotation rates for particles greater than 36 μm decreased for all energy dissipations used. The results for the flotation of moderately hydrophobic quartz are reproduced in Figure 2.11.

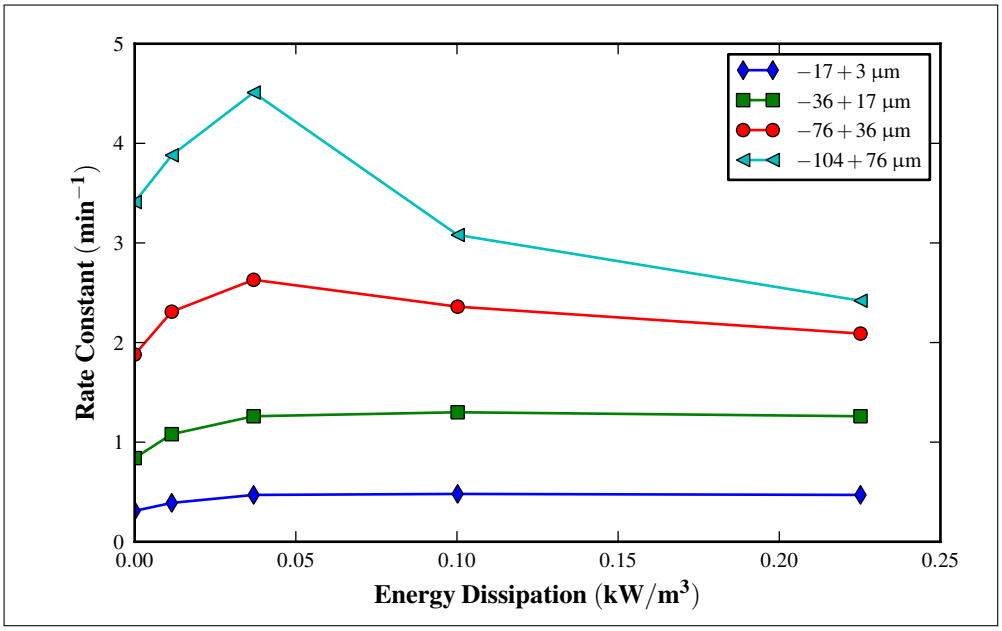

Figure 2.11: Flotation rate constant versus energy dissipation for the flotation of moderately hydrophobic quartz in an oscillatory baffled column, for four particle size classes (adapted from Anderson, 2008).

It is illustrated in Figure 2.11 that the flotation rate constant for sub 36 µm particles increases with increasing energy dissipation, up to approximately 0.05 kW/m^3, beyond which the flotation rate is independent of energy dissipation. Particles greater than 36 µm display optimum flotation rates at an energy dissipation of approximately 0.05 kW/m^3, after which the flotation rate decreases with increasing energy dissipation. This optimum energy dissipation was higher than observed for low hydrophobicity quartz, although it was still an order of magnitude lower than those found using stirred cells (Section 2.5.3.1).

The large difference between the optimum energy dissipation found in the oscillatory baffled column and in stirred cells was proposed by Anderson (2008) to be due to the oscillatory flow imparted on the fluid by the baffles, resulting in an additional fluctuating velocity in the system. This was thought to result in high root mean squared (RMS) velocities in the fluid, leading to high RMS velocities for particles and bubbles at relatively low energy dissipations. It was shown in Section 2.4.2 that increasing the RMS velocities of particles and bubbles results in increased flotation rates. The oscillatory baffled column was therefore speculated to increase particle-bubble contacting

at considerably lower energy dissipations than in conventional cells.

2.5.3.3 Oscillating Grid Cell

The oscillating grid cell (OGC) was developed by Changunda et al. (2008) as a cell which produces near homogeneous and isotropic turbulence. The specifics of the oscillating grid turbulence have been discussed in Section 2.3. Flotation experiments were performed using quartz (P_{80} = 100 µm) which was methylated to an advancing contact angle of 65°. Bubble sizes of 0.13 mm, 0.24 mm and 0.82 mm, and energy dissipations of 0.015 – 0.6 kW/m^3, were used in the investigation. Results for the flotation of the -48 +26 µm particle size class are reproduced in Figure 2.12, for the three bubble sizes used.

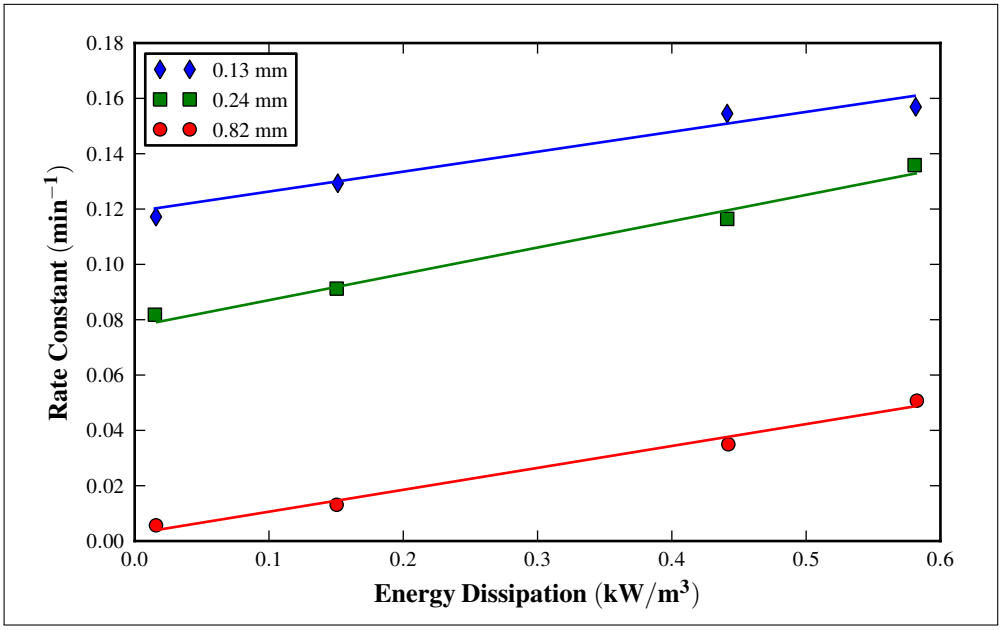

Figure 2.12: Flotation rate constant versus energy dissipation for the flotation of -48 +26 µm quartz in an oscillating grid cell, for three bubble sizes (adapted from Changunda et al., 2008).

Figure 2.12 illustrates that the flotation rate increased linearly with increased energy dissipation (ie. $k \propto \epsilon^1$), for the three bubble sizes used. Similar trends were observed for all particle sizes used in the study. This linear relationship was higher than many theoretical studies have indicated (Nonaka et al., 1982; Julien Saint Amand, 1999),

however, Newell and Grano (2006) noted a similar linear relationship between energy dissipation and flotation rate, in an experimental study. It was observed by Changunda et al. (2008) that the rate of increase in flotation rate with increasing energy dissipation (the slope of the lines in Figure 2.12) was approximately equal for the three bubble sizes used. Similar trends, with regard to changing bubble size, were noted for all particle sizes used. It was therefore proposed that, for the range of energy dissipations and bubbles sizes used, the effect of energy dissipation on flotation rate was not strongly dependent on the bubble size.

In order to discuss the role of particle size on the effect that energy dissipation has on flotation kinetics, the results for the flotation of three particle sizes with 0.24 mm bubbles are reproduced in Figure 2.13.

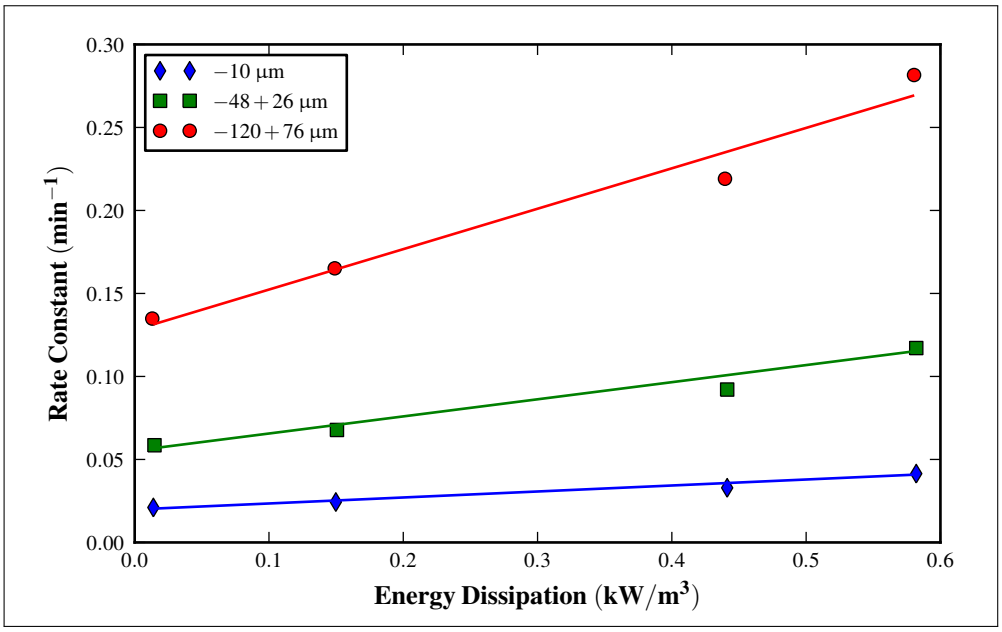

Figure 2.13: Flotation rate constant versus energy dissipation for the flotation of quartz in an oscillating grid cell, for 0.28 mm bubbles and three particle size classes (adapted from Changunda et al., 2008).

Figure 2.13 illustrates that the rate of increase in flotation rate with increasing energy dissipation (the slope of the line) increases with increasing particle size. The effect that energy dissipation has on the flotation kinetics is therefore dependent on the particle size being floated. An exception to this trend was the flotation rates for coarse particles floated with small (0.13 mm) bubbles, where increasing energy dissipation

resulted in flotation rates remaining relatively constant. This effect was attributed to a combination of buoyancy and detachment effects. From these results, Changunda et al. (2008) proposed that the effect of energy dissipation on flotation rate was dependent on the particle size, but was less dependent on the bubble size.

Experiments conducted in stirred cells and the oscillatory baffled column have shown that increasing energy dissipation results in increased flotation rates to an optimum, beyond which the flotation rate decreases with increasing energy dissipation (see Figures 2.8, 2.9 and 2.11). This optimum is thought to be the point where the rate of detachment becomes greater than the rate of increased particle-bubble collisions. It is clear from Figures 2.12 and 2.13 that this optimum is not observed in the oscillating grid cell, indicating that there is negligible detachment occurring in the system. This may be due to the low energy dissipations used in the study. It is proposed that by increasing the energy dissipation, beyond those used by Changunda et al. (2008), the effects of detachment may be observed.

2.5.4 Summary of Experimental Studies

It is evident from the literature that flotation kinetics are a function of many factors, including the particle size, bubble size and energy dissipation in a system. The relationship between flotation rate and particle size can be described by $k \propto d_p^n$, where n is 1 – 1.5 in quiescent systems, and 0.3 – 1 in turbulent sytems. The relationship between the flotation rate and bubble size is commonly described by $k \propto d_b^{-m}$, where m is 1.15 – 3 in quiescent systems, and in the range of 0.75 – 2.2 for turbulent systems.

The effect of increasing energy dissipation is, generally, to increase the flotation rate to an optimum, beyond which increasing the energy dissipation results in decreasing flotation rates. At energy dissipations below the optimum, the relationship between energy dissipation and flotation rate can be described by $k \propto \epsilon^{0.91-1}$. The optimum energy dissipation is in the range of 0.05 – 4.1 kW/m^3, and appears to be a function of bubble size, particle size, particle hydrophobicity and contacting environment. In general the highest flotation rates are achieved when floating with fine bubbles at low energy dissipations.

2.6 Summary of Literature Review

The literature relevant to this investigation has been reviewed in this chapter. The review of flotation cells included common industrial cells, and novel flotation cells which have been developed. It was observed that both operate using turbulent environments, and therefore knowledge of the effects of energy dissipation on flotation may be relevant to both current flotation technology and future developments.

Background information was given on turbulence fundamentals in order highlight the areas important in flotation. Oscillating grid turbulence was then reviewed, demonstrating why they may be considered to provide a near ideal environment for the investigation of turbulent systems.

From the review of theoretical studies of flotation, it was observed that energy dissipation affects flotation in two ways. Firstly increased energy dissipation is thought to increase particle-bubble collision frequencies, resulting in increased flotation rates. This relationship can be expressed as $k \propto \epsilon^{0.44-0.75}$. The second effect of energy dissipation on flotation is to decrease the stability of particle-bubble aggregates. The overall effect that energy dissipation has on flotation kinetics is therefore a balance of these two effects.

The majority of experimental studies on the effect of energy dissipation on flotation kinetics have been conducted in stirred cells, with some research conducted in an oscillatory baffled column and an oscillating grid cell. Studies have shown some general trends regarding the effects of particle size, bubble size and energy dissipation on flotation kinetics. In general, increasing energy dissipation results in increased flotation rates to an optimum, after which the flotation rate decreases with increasing energy dissipation. This optimum is thought to be the point where the rate of detachment becomes greater than the rate of increased particle-bubble collisions, as proposed in the theory. This trend was however not observed in the oscillating grid cell, indicating that the study was limited by the relatively low energy dissipations used. The current study therefore proceeds by using an oscillating grid cell to investigate flotation kinetics at a large range of energy dissipations, such that the effect of energy dissipation on flotation kinetics may be more fully investigated.

Chapter 3

Materials and Methods

In this chapter the materials and methods used in the investigation are presented. A detailed description of the design and operation of the oscillating grid cell is given in Section 3.1. Precharacterisation experiments were conducted in the oscillating grid cell, before flotation experiments could be conducted, and are outlined in Section 3.2. The conditions and procedures for the flotation experiments are then described in Section 3.3, with details of the experimental program for the investigation.

3.1 The Oscillating Grid Flotation Cell

The first objective of this study was to design and build an oscillating grid cell, which could be used at energy dissipations of 0.5 – 5 kW/m^3. The cell was designed to be dimensionally identical to the oscillating grid cells used by Changunda et al. (2008) and Bache and Rasool (2001), but with a more robust design such that higher energy dissipations could be achieved. A schematic of a single grid is shown in Figure 3.1 and the oscillating grid cell is shown in Figure 3.2. The dimensions of the oscillating grid cell and grids are given in Table 3.1

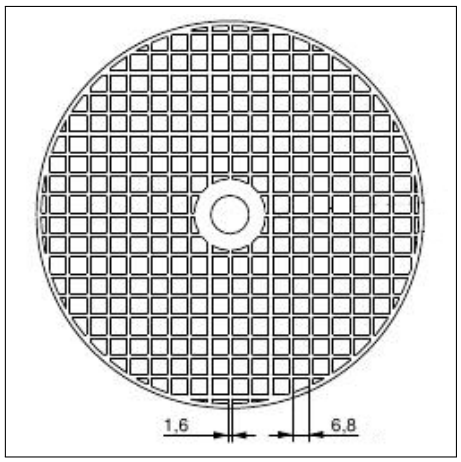

Figure 3.1: Detail of a single grid.

Figure 3.2: The oscillating grid flotation cell.

Table 3.1: Oscillating grid cell specifications.

Volume (L)	10
Tank Height (mm)	380
Tank Width (mm)	180
Number of Grids	19
Grid Spacing (mm)	18
Grid Hole Shape	Square
Grid Hole Size (mm)	6.8
Grids Solids Size (mm)	1.6

The oscillating grid cell was operated by oscillating the grid stack vertically in a PVC column. The grids had the same dimensions as used by Changunda et al. (2008), and were laser cut from single sheets of 1.5 mm stainless steel for added rigidity. A reinforcing ring was added to the circumference of the grids, which was not present in the grids used by Changunda et al. (2008).

The grid stack was made up of 19 grids mounted horizontally on the drive shaft. Turbulence was generated in the system by oscillating the grid stack at a set stroke length of 18 mm, which corresponds to the spacing between the grids. The shaft was oscillated vertically through the use of a crank, which was driven by a variable speed 750 Watt AC Bonfigilioli electric motor. Oscillation frequencies were altered by varying the rotational speed of the motor, and frequencies of 5 – 13 Hz could be achieved using this system. The energy dissipation was altered through changing the oscillating frequency of the grid stack.

3.1.1 Force Measurement

The force was measured by using a load cell (Loadcell Services S-type) mounted in-line on the driving shaft, so as to directly measure the forces exerted on the drive shaft. A small flag mounted on the crank cut an optical switch once a cycle in order to determine the frequency and phase of the crank. Electrical signals were captured using a National Instruments data acquisition card, and sent to a computer where they were saved using LabView© for analysis, which will be described in detail in Section 3.2.

3.1.2 Aeration System

Gas was humidified, by bubbling it through distilled water, before being sparged into the cell through three 30 mm diameter glass frits (Duran sintered filters supplied by Glasstech (Pty) Ltd) situated below the plate stack. The gas flowrate was accurately controlled by using a Brooks Smart (TMF) mass flow controller, before being distributed to the spargers. The frits were mounted in stainless steel pipes which could be rotated through 180 degrees, as shown in Figure 3.3.

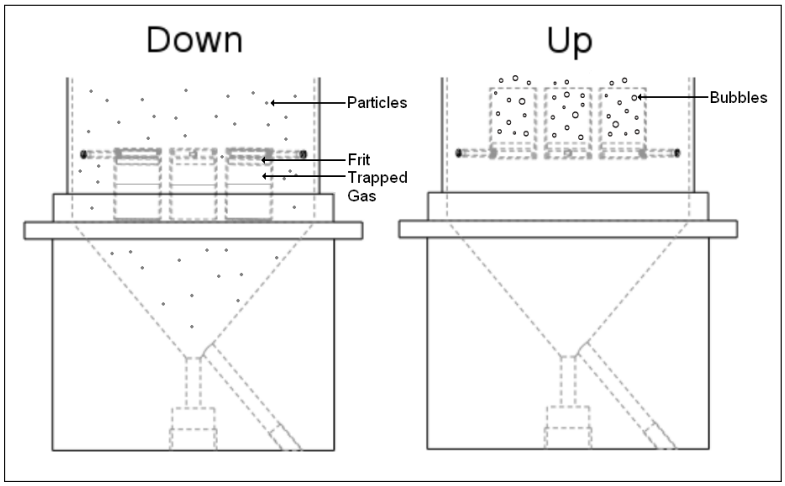

Figure 3.3: Schematic of frit placement with detail of rotation.

When in the "down" position the frits were protected from being clogged with settling particles, and when the gas was turned on it was trapped in the pipe. When rotated to the "up" position the air was allowed to escape. Porosity 1, 3 and 4 frits were used, which produce known bubble sizes as measured by Deglon (1998). Table 3.2 shows the maximum pore size of the different porosity frits, with the mean bubble size produced. Deglon (1998) found that at the energy dissipations used in this study, and with the same frother dosage, bubble break-up is negligible.

Table 3.2: Sintered glass frit pore sizes and corresponding mean bubbles sizes produced, as measured by Deglon (1998).

Porosity	Max Pore Size (μm)	Mean Bubble Size (mm)
1	100 - 160	0.82
3	16 - 40	0.24
4	10 - 16	0.13

3.1.3 Recycle System

The flotation experiments were run in batch mode, and a recycle was therefore required to keep the particles sufficiently dispersed. The column was fitted with a conical base so that slurry could be collected and continuously reintroduced to the top of the cell. A small centrifugal pump (Boyu S-1800) was used so as to maintain a constant flow of 4.5 L/min. The piping had few obstructions and had a suitably large diameter to ensure laminar flow.

3.1.4 Froth Removal System

In order to minimise froth recovery effects a very low froth was maintained, which was removed by skimming a vacuum nozzle, attached to a conical flask, across the liquid surface. This method has been used by many previous researchers (Ahmed and Jameson, 1985; Deglon, 1998; Changunda et al., 2008; Anderson, 2008). Five separate concentrates could be collected using this system.

3.2 Precharacterisation Experiments

The precharacterisation of the oscillating grid cell was composed of two parts, the determination of the energy dissipation in the system, and the comparison to Changunda et al. (2008) who conducted research in a similar rig. The comparison to previous work was conducted by floating the same methylated quartz as used by Changunda et al. (2008), and is therefore referred to as the methylated quartz flotation.

3.2.1 Determination of Energy Dissipation

The method described in this section, to determine the energy dissipation in the oscillating grid cell, follows that of Bache and Rasool (1996). The force measured by the load cell was composed of a combination of forces, namely, the force required to accelerate the grids, frictional force in the mechanism and the force exerted by the grids on the fluid. In order to determine the force exerted by the grids on the fluid, the force was measured with no fluid in the cell (F_{dry}) and then with fluid (F_{wet}), as described by Tojo et al. (1979). The force exerted on the fluid was then calculated by:

$$F(t) = F(t)_{wet} - F(t)_{dry} \tag{3.1}$$

The instantaneous power supplied to the fluid at time (t) was then calculated by:

$$P(t) = F(t)\dot{Y}(t) \tag{3.2}$$

where the instantaneous velocity $\left(\dot{\mathrm{Y}}(\mathrm{t})\right)$ was given by:

$$\dot{Y}(t) = \pi S f sin(2\pi f t) \tag{3.3}$$

where S is the stoke (18 mm) and f is the frequency of oscillation. The time-averaged power input ($\overline{\mathrm{P}}$) was then calculated from:

$$\overline{P} = \frac{1}{\tau}\int_0^\tau P(t)dt \tag{3.4}$$

where τ is the period of oscillation and is equal to f^{-1}. The average rate of energy dissipation ($\overline{\epsilon}$) was then calculated by:

$$\overline{\epsilon} = \frac{\overline{P}}{m_L} \tag{3.5}$$

where m_L is the mass of liquid in the agitated zone. The energy dissipation can be expressed as power intensity (kW/m^3), specific power input (W/kg) or turbulent en-

ergy dissipation rate (W/kg or m^2/s^3), which are considered to be equivalent under the conditions used in this investigation (Changunda et al., 2008).

3.2.2 Methylated Quartz Flotation

The aim of the methylated quartz flotation experiments was to show continuity from the work done by Changunda et al. (2008). This was achieved by repeating the experiments conducted by Changunda et al. (2008) in the new oscillating grid cell, and comparing the results obtained with the results of Changunda et al. (2008). The same methylated quartz that was prepared and floated by Changunda et al. (2008) was reused for these experiments, and was floated at identical operating conditions. It should be noted that the quartz had been in storage for approximately 18 months prior to being reused in this study. Further details of the ore preparation and operating conditions used can be found in Changunda et al. (2008). For the experiments an energy dissipation of 5 kW/m^3 was used, which is within the range of energy dissipations used by Changunda et al. (2008).

3.3 Flotation Experiments

This section will provide the details of the ore sample used in the flotation experiments, followed by the operating conditions used in the flotation experiments. The procedures used for a flotation experiment are then described in detail.

3.3.1 Ore Sample

Quartz has been used extensively in flotation research as it does not undergo oxidation and can easily be rendered hydrophobic, either through adding collector or methylation techniques. In this study, natural quartz was floated using a collector in order to produce results comparable to those of Deglon (1998) and Anderson (2008). The quartz sample (supplied by Kiln Contracts (Pty) Ltd, Western Cape) was used as supplied without further milling. The particle size distribution of the sample, as measured using a Malvern Mastersizer^{TM}, is shown in Figure 3.4.

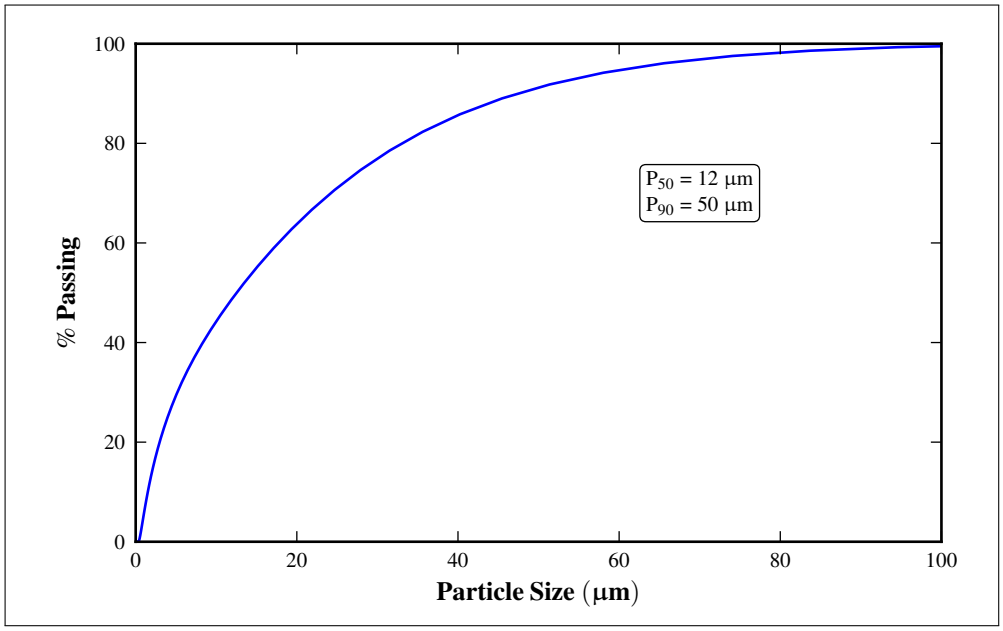

Figure 3.4: Size distribution of natural quartz sample used in this study.

It is illustrated in Figure 3.4 that the sample had a large percentage of fine and ultra-fine material, which may be more typical of a milled ore. The focus of the investigation is on the flotation of fine particles, since they float poorly and are generally thought to benefit from energy dissipation. The large percentage of fine particles in the ore sample is therefore well suited to the study. This sample was blended and split, using a spinning riffler, into feed samples for the flotation experiments.

3.3.2 Experimental Conditions

Flotation experiments were conducted in batch mode, using constant flotation conditions for all experiments. These operating conditions are summarised in Table 3.3.

Table 3.3: Table of experimental conditions for flotation experiments.

Gas	N_2
Gas Flow (mL/min)	100
Solid Concentration (mass %)	0.5
Frother	MIBC
Frother Concentration (ppm)	100
Sampling Times (min)	0.5, 1, 2, 4, 8

Nitrogen gas (Air Liquide Analytical grade) was used as the flotation gas. Low gas flowrates were used in order to minimise the effect that bubbles might have on the turbulence in the system. A low mass percentage of solids was used so as to minimise the effect that solids may have on the turbulence, and to minimise bubble loading. MIBC (Fluka 97.5 %) was used at the same concentrations as Deglon (1998) and Changunda et al. (2008), so as to produce the same bubble sizes as those studies. The collector used was dodecylamine (Fluka 98 %) at a dosage of 1 x 10^{-4} mol/L at pH 9. At this collector concentration a maximum recovery of up to 90 % was achieved over the 8 minute flotation time period.

3.3.3 Experimental Procedures

This section describes, in detail, how an experiment in the oscillating grid cell was carried out. Before the experiment began, the oscillating frequency corresponding to the desired energy dissipation to be used was set on the motor. To begin with, the spargers were set up facing downwards and with no Nitrogen flow, and the cell was filled with water. Frother and collector were pre-dispersed in beakers of water, and added to the cell. The oscillating grid and recycle pump were then started, and allowed to operate for 2 min in order to mix the reagents throughout the cell. The ore was then introduced as a slurry beneath the water surface, in order to reduce air entrainment. After 10 min of conditioning time the Nitrogen gas was started,

and allowed to run for 15 seconds to reach steady state. Since the spargers were facing down this Nitrogen gas was trapped, as shown in Figure 3.3. After 15 seconds the spargers were turned to face upwards, and once the slugs of Nitrogen gas had risen to the surface the timer was started for the flotation tests. Five concentrates were collected in separate conical flasks, for the flotation times given in Table 3.3. The concentrates were dried, weighed, and the size distributions determined using a Malvern Mastersizer^{TM}. From this data the mass of each particle size class, in every concentrate, was calculated. The flotation rate constant (k) was then calculated using curve fitting for each particle size class by:

$$R(t) = 1 - e^{-kt} \tag{3.6}$$

where the recovery (R) is the fraction of the feed that is recovered at time t.

3.3.4 Experimental Program

The experimental program for this study was composed of two major parts, the precharacterisation of the oscillating grid cell, and the flotation experiments conducted in order to investigate the effect of energy dissipation on flotation kinetics. The experiments performed, in both the precharacterisation and the flotation experiments, are summarised in Table 3.4, with further detail given in Sections 3.3.4.1 – 3.3.4.2.

Table 3.4: Table of summarised experiments conducted in the oscillating grid cell.

Experiment	**Ore**	**Energy Dissipation (kW/m^3)**	**Bubble Size (mm)**
Comparison to Changunda et al. (2008)	Methylated Quartz	0.5	0.13, 0.24, 0.82
Repeatability	Natural Quartz	0.5, 1, 2, 3, 4, 5	0.24
Flotation Experiments	Natural Quartz	0.5, 1, 2, 3, 4, 5	0.13, 0.24, 0.82

3.3.4.1 Precharacterisation Experiments

Before flotation experiments were conducted in the cell, the energy dissipation in the cell was determined at oscillating frequencies of 2 Hz, 5 Hz, 7 Hz, 10 Hz and 13 Hz. A calibration curve was then drawn, which allowed the appropriate oscillating frequency to be chosen to produce a desired energy dissipation.

Flotation of methylated quartz was performed in order to benchmark the cell against the results of Changunda et al. (2008), and to ensure that the oscillating grid cell was operating as expected. These experiments were conducted using the same operating conditions and methylated quartz as Changunda et al. (2008). An energy dissipation of 0.5 kW/m^3 was used for the experiments, as it falls in the range of 0.015 – 0.65 kw/m^3 used by Changunda et al. (2008), and was the lowest energy dissipation which could be achieved in the oscillating grid cell.

The repeatability of the results obtained in the oscillating grid cell was determined by performing flotation experiments in duplicate, using natural quartz, at the operating conditions given in Table 3.4.

3.3.4.2 Flotation Experiments

Natural quartz flotation experiments were conducted in the oscillating grid cell at the conditions shown in Table 3.4. The energy dissipations used were chosen to cover a large range, including the dissipations which may be of interest to industry. The bubble sizes may be considered small in terms of industry use, however they correspond to the range typically used in the literature, to which results from this study will be compared (Ahmed and Jameson, 1985; Deglon, 2002; Anderson, 2008; Changunda et al., 2008). The results of these experiments allowed observations to be made on the effect of energy dissipation on flotation kinetics, these are presented and discussed in Chapter 4.

Chapter 4

Results and Discussion

This chapter is presented in three sections, beginning with the precharacterisation of the new oscillating grid cell, in Section 4.1. The results from the quartz flotation experiments done in the oscillating grid cell are then presented in Section 4.2. These results are discussed in terms of the effects of bubble size, particle size and energy dissipation on flotation kinetics. The chapter concludes in Section 4.3, with a brief discussion on the effect of the contacting environment on flotation kinetics, with reference to previous literature studies conducted in a stirred cell and an oscillatory baffled column.

4.1 Precharacterisation of the Oscillating Grid Cell

The precharacterisation of the oscillating grid cell was composed of three parts, the energy dissipation measurements, the comparison to previous research in a similar rig, and the repeatability of the data acquired from experiments. The results from these precharacterisation experiments are presented and discussed in this section.

4.1.1 Energy Dissipation Measurements

Energy dissipation measurements were conducted as described in Section 3.2. It was found that the presence of bubbles and solids, at low gas flow rates and solids con-

centrations, had a negligible effect on the energy dissipation, and therefore the results presented are applicable for the flotation experiments. The measured instantaneous power input into the fluid, with relation to the grid velocity, is shown in Figure 4.1, for a grid oscillating frequency of 13 Hz.

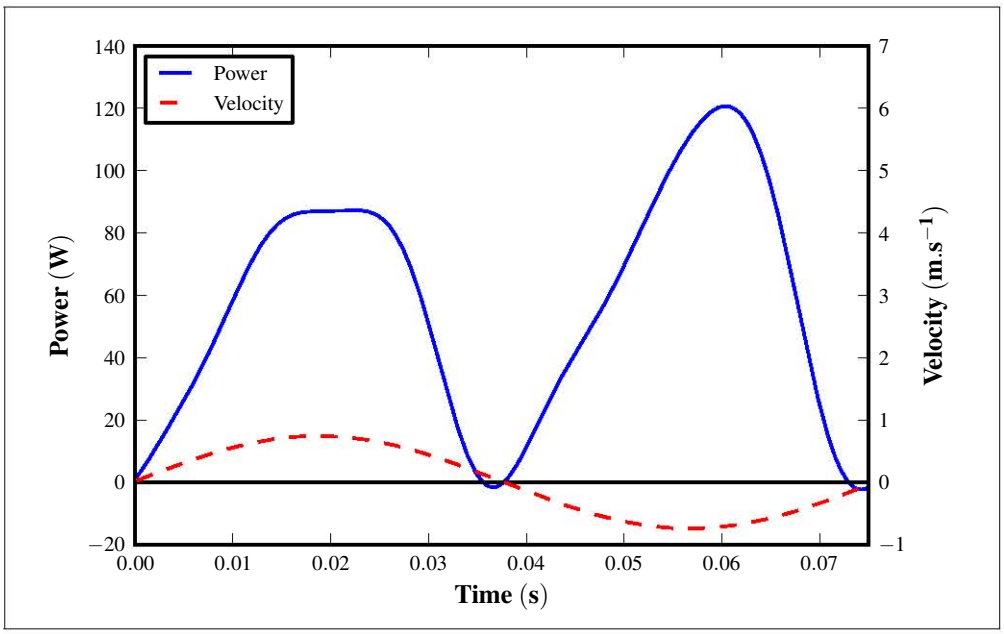

Figure 4.1: Measured instantaneous power input at 13 Hz, in relation to grid velocity.

Figure 4.1 illustrates that the instantaneous power input is directly related to the grid velocity, reaching maximum values when the grid velocity is at a maximum, and zero when the grid is stationary (velocity = 0 m/s). This is due to the fact that the power being input into the system comes from the frictional force exerted by the grids, which is directly related to the velocity of the grids. The grids are essentially moving through a stationary fluid, which is expected since oscillating grid turbulence is considered to be zero mean flow (Yan et al., 2007). This is the significant difference between the oscillating grid cell and an oscillatory baffled column, which has high levels of bulk fluid flow.

The average energy dissipation rate ($\overline{\epsilon}$) was described by the relationship given by Guadayol et al. (2009)

$$\overline{\epsilon} = \frac{n\frac{2}{3}C_d\rho_f\pi^2 S_A f^3 S^3}{m_L} \tag{4.1}$$

where the drag coefficient (C_d) was found to be constant and equal to 4.55, after curve fitting with the experimental data. In the current system the number of grids (n), fluid density (ρ_f), mass of fluid being agitated (m_L), solids area of the grids (S_A) and oscillating stroke length (S) are all constant, and the energy dissipation is manipulated by changing the oscillating frequency (f). This relationship between grid oscillating frequency and average energy dissipation is shown in Figure 4.2, for both the experimental and fitted data.

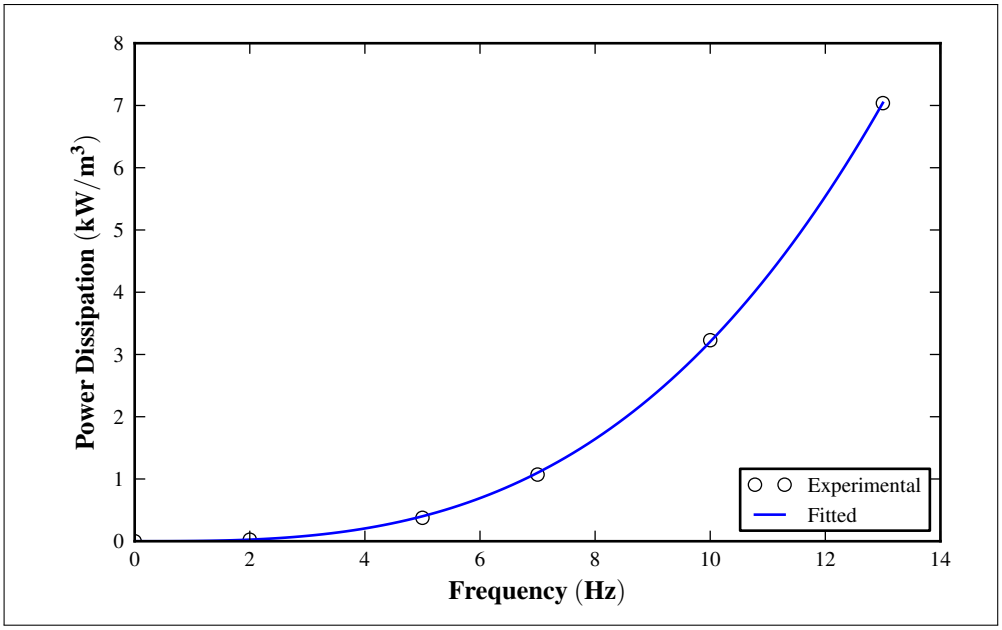

Figure 4.2: Energy dissipation versus grid oscillating frequency, experimental results with fitted curve corresponding to Equation 4.1.

It is clear from Figure 4.2 that the equation is a good fit to the experimental data, for the range of frequencies used. Equation 4.1 was therefore used to back calculate the oscillating frequencies to be used in the flotation experiments. Table 4.1 shows the energy dissipations used in the study, with the grid oscillating frequencies required to achieve them.

Table 4.1: Operating frequencies with corresponding energy dissipations.

Frequency (Hz)	Energy Dissipation (kW/m^3)
5.4	0.5
6.7	1
8.5	2
9.8	3
10.8	4
11.7	5

4.1.2 Methylated Quartz Flotation

The same methylated quartz as used by Changunda et al. (2008) was floated in order to ensure that the new cell had similar flotation behaviour to the cell used by Changunda et al. (2008). The flotation results from the current study and from Changunda et al. (2008) are compared in Figures 4.3 and 4.4, for the flotation of three particle size classes using 0.82 mm and 0.13 mm bubbles.

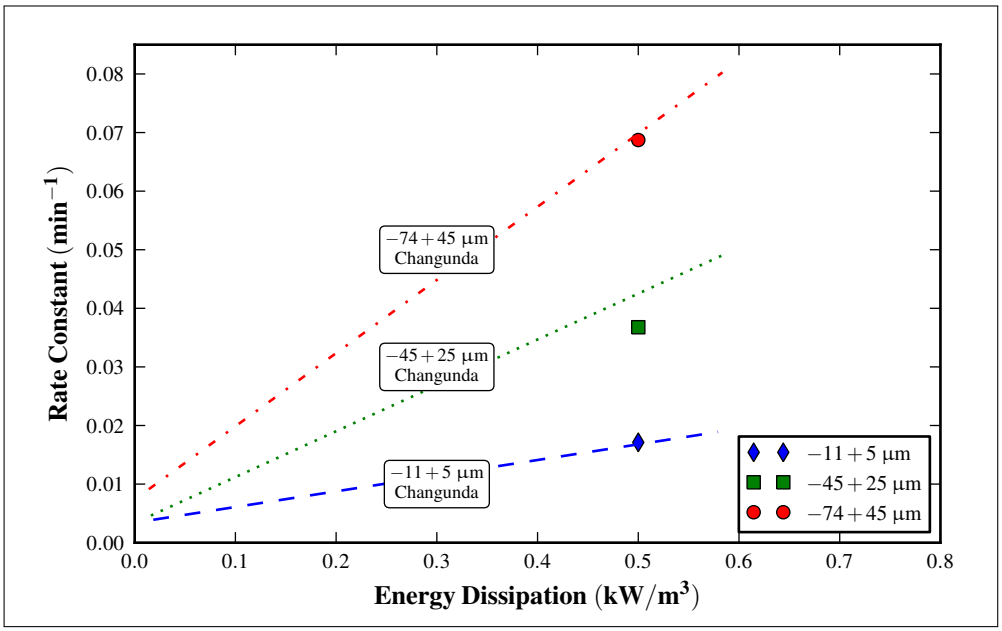

Figure 4.3: Flotation kinetics for increased energy dissipation, using 0.82 mm bubbles. Lines represent results from Changunda et al. (2008), whilst closed symbols are the results from the current study.

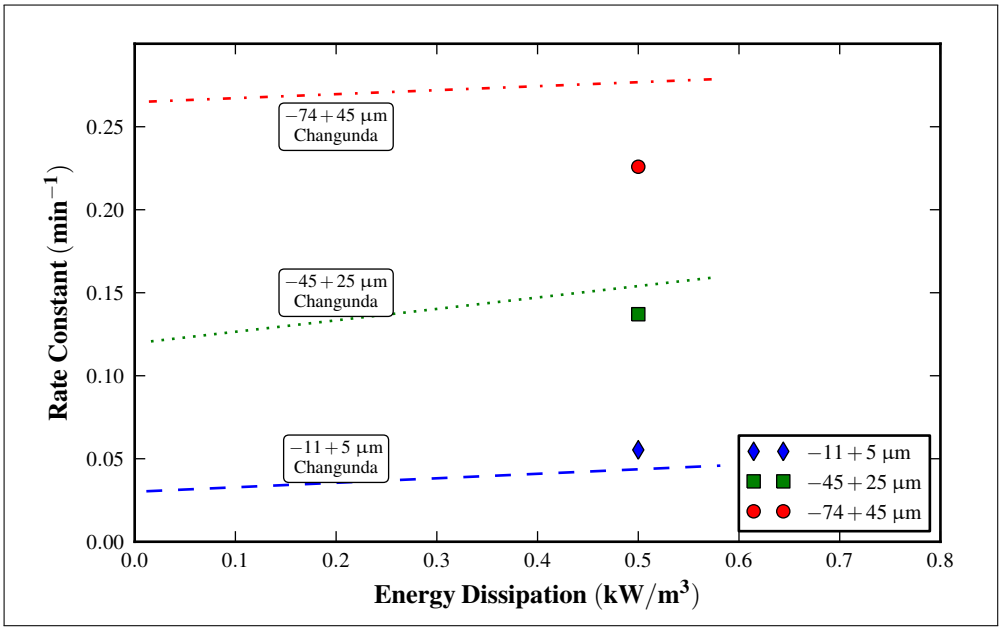

Figure 4.4: Flotation kinetics for increased energy dissipation, using 0.13 mm bubbles. Lines represent results from Changunda et al. (2008), whilst closed symbols are the results from the current study.

Figure 4.3 illustrates that the flotation experiments, when using 0.82 mm bubbles, show good agreement between the results from Changunda et al. (2008) and the current study at 0.5 kW/m^3, for the three particle size classes. Figure 4.4 shows that, for flotation with 0.13 mm bubbles, there is good agreement for the -11 +5 µm and the -45 +25 µm particle size classes. However, the results for the largest particle size class (-74 +45 µm) do not match as closely. Large particles floated with small bubbles are expected to experience high detachment forces, and therefore this discrepancy may indicate that the quartz had lost some hydrophobicity during storage. If one considers that the oscillating grid cell used in the current study was a new cell, with differences in the grid design (see Section 3.1), and was used by a different operator, then it may be considered to operate at a satisfactorily equivalent manner to the cell used by Changunda et al. (2008).

4.1.3 Repeatability

The repeatability of the results obtained using the oscillating grid cell was determined by performing quartz flotation experiments in duplicate, using 0.24 mm bubbles, for energy dissipations of 0.5 kW/m^3, 1 kW/m^3, 2 kW/m^3, 3 kW/m^3, 4 kW/m^3 and 5 kW/m^3. The percentage error between repeats was averaged over all experiments, and is given in Table 4.2, for both the recovery and calculated rate constant.

Table 4.2: Average errors for recovery and flotation rate constant.

	Relative Error (%)	
Size Fraction (μm)	**Recovery**	**Rate Constant**
-19 +5	5.4	6.4
-45 +19	4.9	5.6
-74 +45	4.3	5.0

Similar errors have been reported by Changunda et al. (2008), where errors of approximately 5 % were found for recovery in a similar system. These errors were considered to be in a reasonable range for these experiments, and are used as a standard throughout the study.

4.2 Flotation in the Oscillating Grid Cell

In this section the flotation experiments outlined in Section 3.3, for the flotation of natural quartz in the oscillating grid cell, are presented and discussed. The results are initially discussed in terms of particle and bubble size, at low energy dissipation. This is done in order to demonstrate that the oscillating grid cell had flotation behaviour which is as expected, and is comparable to literature findings. The effect that increasing the energy dissipation has on flotation kinetics is then presented, with discussion on the roles of both bubble and particle size.

4.2.1 The Effect of Particle and Bubble Size on Flotation Kinetics

The relationship between flotation rate and particle size, at an energy dissipation of 0.5 kW/m^3, is presented in Figure 4.5, for the three bubble sizes used in the investigation.

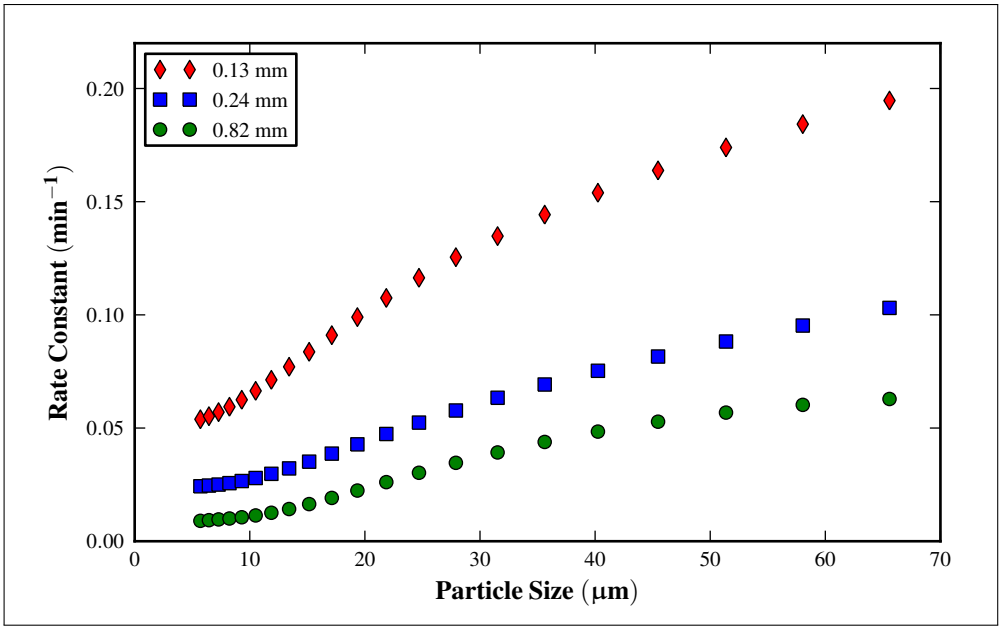

Figure 4.5: Flotation rate constant versus particle size at 0.5 kW/m^3, for all bubble sizes.

It is clear from Figure 4.5 that the flotation rate increases with increasing particle size, for the range of particle sizes and bubble sizes used. This relationship is well established in the flotation literature, and is commonly expressed as $k \propto d_p^n$. In this

study the value of n was calculated to be approximately 0.7. This relationship was not as strong as observed in the literature for quiescent systems, where the value of n is considered to be in the range 1 – 1.5 (Jameson et al., 1977; Crawford and Ralston, 1988). Literature studies in turbulent systems indicate that the relationship decreases when agitation is applied (Ahmed and Jameson, 1985, 1989), and in general n is in the range 0.38 – 1 for turbulent systems (Gaudin et al., 1942; Trahar, 1981; Deglon, 1998; Pyke et al., 2003; Changunda et al., 2008). The value of n found in this study was in this range, and the relationship between particle size and flotation rate was therefore considered to be consistent with the literature for turbulent systems.

The relationship between bubble size and the flotation rate, at an energy dissipation of 0.5 kW/m^3, is shown in Figure 4.6, for three particle size classes.

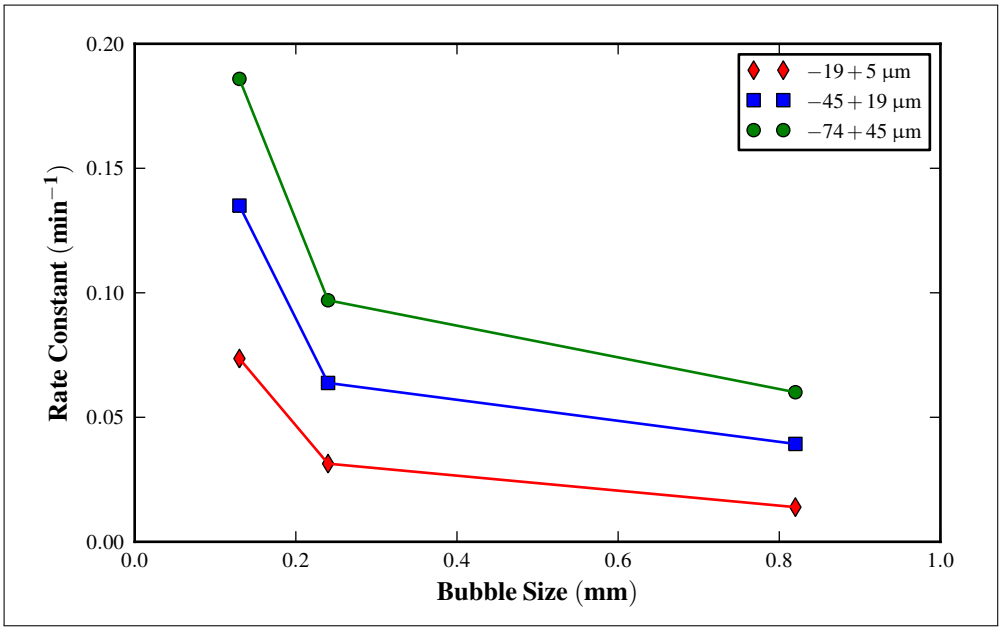

Figure 4.6: Flotation rate constant versus bubble size at 0.5 kW/m^3, for three particle size classes.

Figure 4.6 illustrates that the flotation rate constant increases significantly with decreased bubble size. This relationship is commonly accepted in the literature, and can be described by the inverse power relationship $k \propto d_b^{-m}$. In this study the value of m was found to be approximately 0.9. For flotation in quiescent systems the value of m has been reported to be in the range 1.15 – 3 (Jameson et al., 1977; Yoon and Luttrell, 1986; Diaz-Penafiel and Dobby, 1994). In turbulent systems the relationship is not as

strong (Ahmed and Jameson, 1985), and values of m from 0.75 – 2.2 have been reported (Deglon, 1998; Julien Saint Amand, 1999; Changunda et al., 2008). The value of m found in this study falls in the range for turbulent systems. The effect of bubble size on flotation kinetics, at low energy dissipation, was therefore considered to be in good agreement with the literature.

These results indicated that, as a flotation device, the new oscillating grid cell was operating as expected for the flotation of quartz, since the flotation results were consistent with those observed in the literature.

4.2.2 The Effect of Energy Dissipation on Flotation Kinetics

In this section the effect that energy dissipation had on flotation kinetics is presented and discussed. The effect of increasing energy dissipation on flotation kinetics, with regard to particle size, is shown in Figure 4.7, for flotation with 0.24 mm bubbles.

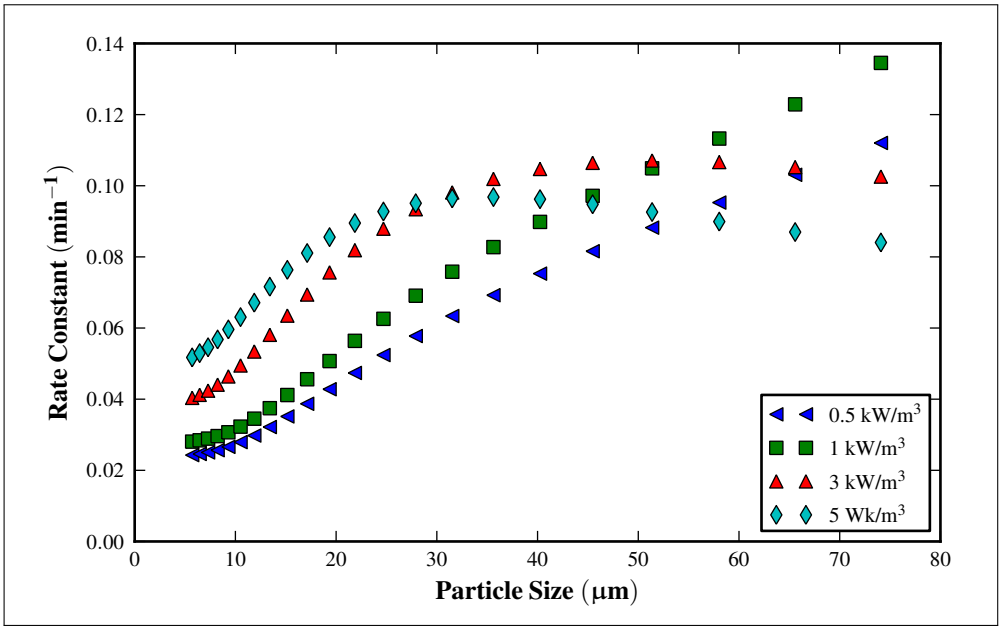

Figure 4.7: Flotation rate constant versus particle size, for flotation with 0.24 mm bubbles at 0.5 kW/m^3, 1 kW/m^3, 3 kW/m^3 and 5 kW/m^3.

Figure 4.7 illustrates that at low energy dissipation (0.5 kW/m^3) the flotation rate increases with particle size, for the range of particle size used. Increasing the energy

dissipation to 1 kW/m^3 results in increasing flotation rates for all particle sizes. Subsequent increases in energy dissipation (3 kW/m^3 and 5 kW/m^3) results in decreasing flotation rates for more coarse particles, whilst fine particle flotation rates increase. Intermediate particle sizes appear to stay reasonably constant. It is clear from Figure 4.7 that the effect of energy dissipation on flotation kinetics is strongly dependent on the particle size. The flotation results have therefore been divided into three particle size classes, namely, -19 +5 µm (fine), -45 +19 µm (intermediate) and -74 +45 µm (coarse), for further discussion. It is acknowledged that the "coarse" particles are not coarse by conventional flotation standards, however the terminology is used in this discussion for convenience.

4.2.2.1 Fine Particles

The effect of energy dissipation on the flotation rate of fine particles (-19 +5 µm) is depicted in Figure 4.8, for flotation with the three bubble sizes used in the study.

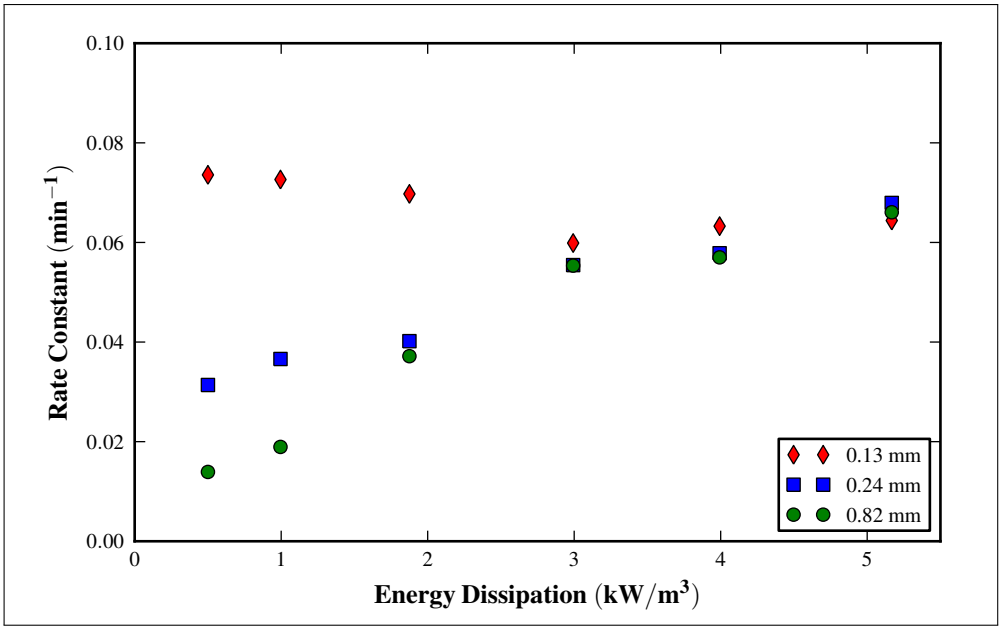

Figure 4.8: Flotation rate constant versus energy dissipation, for the flotation of fine particles (-19 +5 µm) and all bubble sizes.

Figure 4.8 illustrates that at low energy dissipation the flotation rate is inversely dependent on the bubble size, as was discussed in Section 4.2.1. When floating with bubbles

near the size typically found in industry (0.82 mm), increasing the energy dissipation from 0.5 – 5 kW/m^3 results in the flotation rates increasing almost linearly, with a total increase of approximately 500 %. The flotation rates when using fine bubbles (0.13 mm) are high, at low energy dissipation, whilst increasing the energy dissipation results in the flotation rate remaining relatively constant. The flotation rates for flotation with 0.24 mm bubbles lie between the flotation rates when using 0.13 mm and 0.82 mm bubbles. It is observed that at higher energy dissipations (above 3 kW/m^3) the flotation rate is essentially independent of bubble size.

4.2.2.2 Intermediate Particles

The effect of energy dissipation on the flotation rate of the intermediate particle size class (-45 +19 µm) is depicted in Figure 4.9, for the three bubble sizes used in the study.

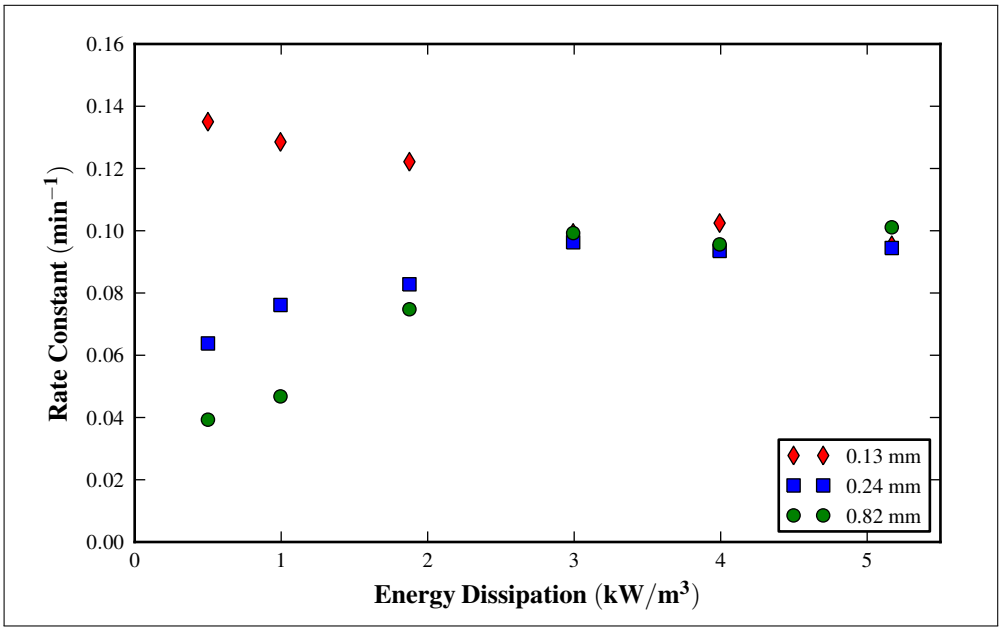

Figure 4.9: Flotation rate constant versus energy dissipation, for the flotation of intermediate particles (-45 +19 µm) and all bubble sizes.

Figure 4.9 illustrates that the intermediate particle size has flotation rates which are generally greater than those for fine particles (Figure 4.8). Flotation when using typical industry sized (0.82 mm) bubbles results in the flotation rate increasing with in-

creasing energy dissipation up to 3 kW/m^3, after which the flotation rate is relatively constant with increasing energy dissipation. Flotation rates increased by approximately 250 %, this is less than observed for fine particles, which increased by 500 % when floated with the same bubble size. Flotation with fine (0.13 mm) bubbles leads to decreased flotation rates with increased energy dissipation, for all energy dissipations used. Medium sized (0.24 mm) bubbles have flotation rates which lie in between those of 0.13 mm and 0.82 mm bubbles. At energy dissipations above 3 kW/m^3 the flotation rate is independent of the bubble size.

4.2.2.3 Coarse Particles

The effect of energy dissipation on the flotation rate of coarse particles (-74 +45 μm) is depicted in Figure 4.10, for the three bubble sizes used in the study.

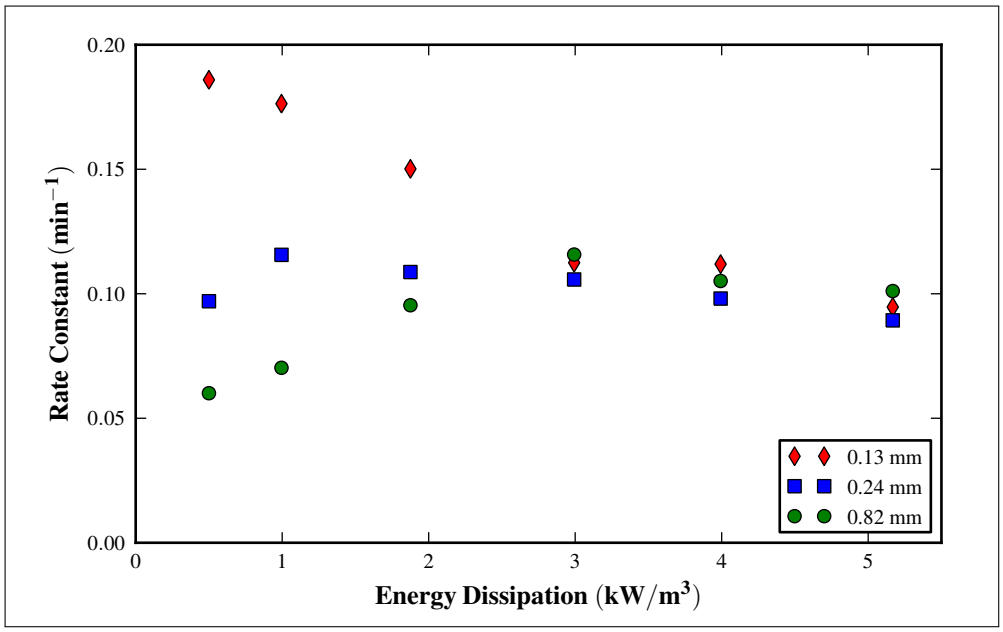

Figure 4.10: Flotation rate constant versus energy dissipation, for the flotation of coarse particles (-74 +45 μm) and all bubble sizes.

Figure 4.10 illustrates that for coarse particles the flotation rates are higher than those for the finer particle sizes (Figures 4.8 and 4.9). Flotation with 0.82 mm bubbles results in the flotation rate increasing two fold when the energy dissipation is increased from 0.5 – 3 kW/m^3, after which the flotation rate decreases. When 0.24 mm bubbles

are used the flotation rate increases with increasing energy dissipation, to a maximum at approximately 1 kW/m^3. Flotation rates when using fine (0.13 mm) bubbles decrease sharply with increasing energy dissipation, halving in value when the energy dissipation is increased from 0.5 – 5 kW/m^3.

4.2.2.4 Summary

The relationship between the flotation rate constant and energy dissipation, for all bubble and particle sizes, is summarised in Figure 4.11. The results have been separated into the three particle size classes as discussed in Sections 4.2.2.1 – 4.2.2.3.

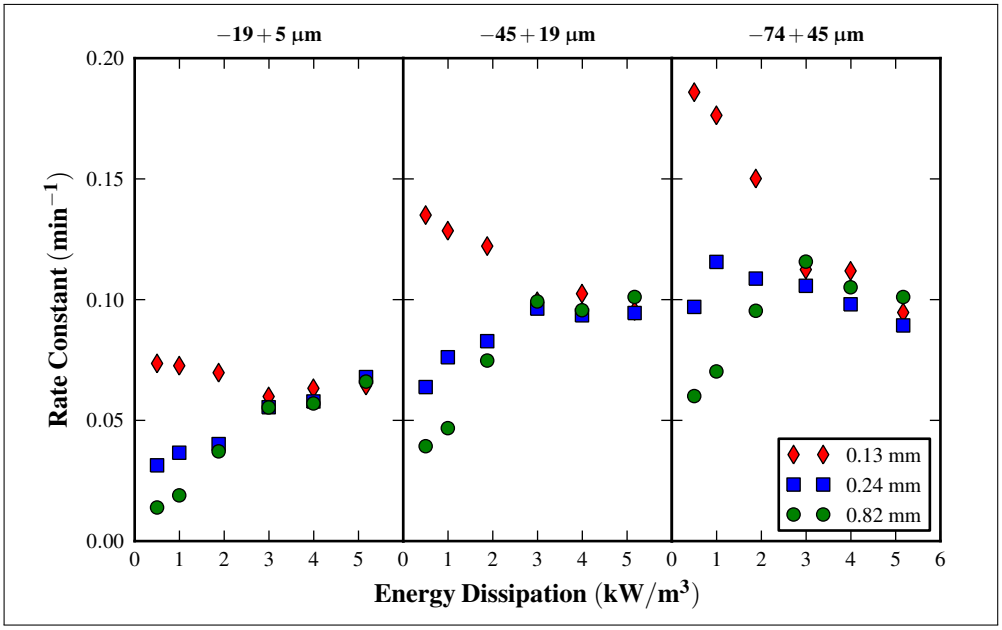

Figure 4.11: Flotation rate constant versus energy dissipation, for all bubble and particle sizes.

Figure 4.11 illustrates the effects of particle size, bubble size and energy dissipation on the flotation rate, and some key findings can be noted. For flotation with industry sized (0.82 mm) bubbles, fine particle flotation rates increase when increasing the energy dissipation from 0.5 – 5 kW/m^3, however for coarse particles increasing the energy dissipation is beneficial only to 3 kW/m^3, after which the flotation rate decreases. When fine (0.13 mm) bubbles are used, the flotation rates of fine particles remain

relatively constant with increased energy dissipation, whilst coarse particle flotation rates decrease significantly with increased energy dissipation.

It is difficult to discern from Figure 4.11 what the magnitude of the effect that energy dissipation has on flotation rates is, for the various bubble sizes and particle size classes. The percentage increase in flotation rate relative to the flotation rate at 0.5 kW/m^3, for each bubble size and particle size class, has therefore been calculated, and is illustrated in Figure 4.12.

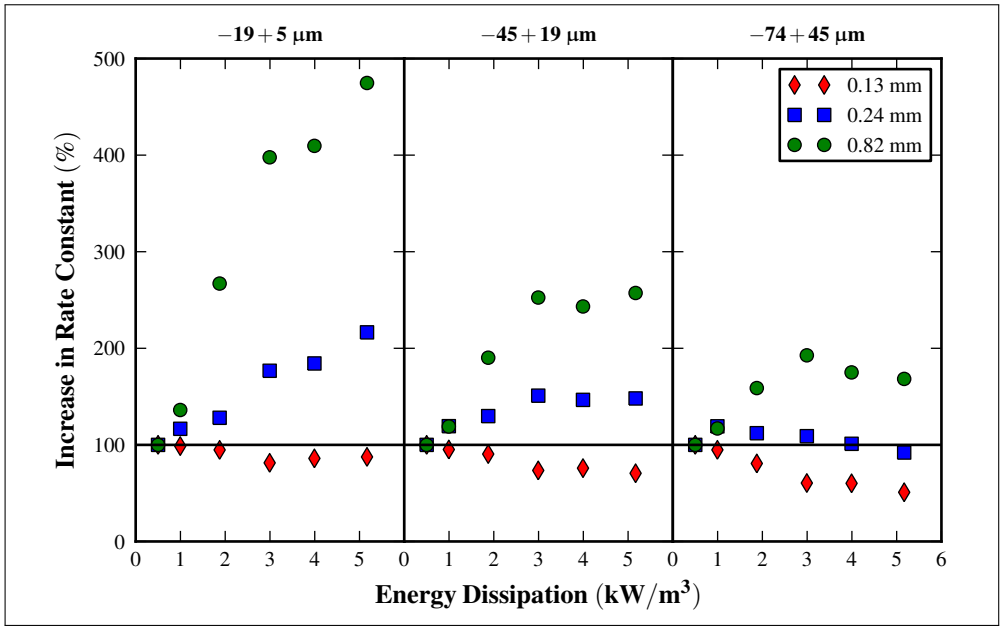

Figure 4.12: Percentage change in the flotation rate constants, relative to the rate at low energy dissipation (0.5 kW/m^3), versus energy dissipation, for all bubble and particle sizes.

Figure 4.12 illustrates that the flotation rates for fine particles, when floated with 0.82 mm bubbles, are the most affected by increasing energy dissipation, where the flotation rate is increased by 500 % when increasing the energy dissipation from 0.5 – 5 kW/m^3. The flotation rate of intermediate particles increases by 250 %, whilst for coarse particles the flotation rate increases by a maximum of 200 %. Flotation rates for the flotation with 0.24 mm bubbles increase by a maximum of 200 %, for the fine particle size class, whilst the flotation rates for the coarse particle size class are relatively unchanged with increasing energy dissipation. The flotation rates for the flotation with 0.13 mm bubbles decrease for all conditions, with the largest decrease

occurring for the coarse particle size class. These results indicate that the dependence of the flotation rate on energy dissipation decreases with decreasing bubble size and increasing particle size. Fine particles floated with large bubbles therefore benefit the most from increased energy dissipation.

Higher flotation rates with increased energy dissipation are proposed to be due to increased collision frequencies between particles and bubbles. Increasing energy dissipation may also lead to increased detachment of particles from bubbles, which may account for decreasing flotation rates with increased energy dissipation. From the results presented, it would appear that detachment rates increased with decreasing bubble size and increasing particles size. These observations are consistent with experimental studies in the literature (Ahmed and Jameson, 1985, 1989; Deglon, 1998), as well as the general trends expected from fundamental theories for collision rates (Section 2.4.2) and the Schulze model for detachment (Section 2.4.1.3).

The relationship between flotation rate and energy dissipation can be described as k $\propto \epsilon^N$, if it is assumed that collision and attachment efficiencies are independent of energy dissipation, and that there is no detachment. It has been seen that fine particles floated with 0.24 mm and 0.82 mm bubbles were the least susceptible to detachment in this study, therefore only these results were used for the determination of N. These results are shown in Figure 4.13, with the value of N given.

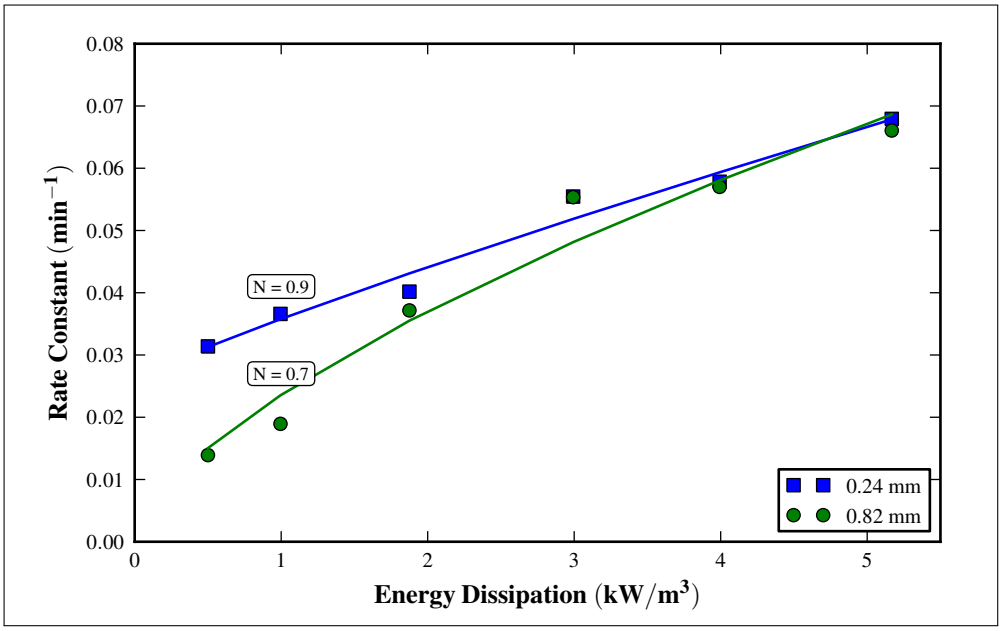

Figure 4.13: Flotation rate constant versus energy dissipation, for the flotation of fine particles (-19 +5 μm) and 0.23 mm and 0.84 mm bubbles. Solid lines represent the fitted equation to the form $k \propto \epsilon^N$, with the value of N shown.

It is illustrated in Figure 4.13 that, for fine particles floated with 0.84 mm and 0.24 mm bubbles, the floating rate increases with increasing energy dissipation. The rate at which the flotation rate increases with increased energy dissipation (the "slope" of the lines) is dependent on the bubble size, with flotation rates for 0.82 mm bubbles increasing a higher rate. The value of N was found to be 0.9 and 0.7, for flotation with 0.24 mm and 0.82 mm bubbles respectively. For comparative purposes, the values of N obtained in theoretical and experimental studies are presented in Table 4.3.

Table 4.3: Values for the constant N in the relationship $k \propto \epsilon^N$, as found in theoretical and experimental studies.

Theoretical		**Experimental**	
Nonaka et al. (1982)	0.75	Nonaka et al. (1982)	0.75
Julien Saint Amand (1999)	0.44 – 0.5	Deglon (2002)	0.91
Pyke (2004)	0.44	Newell and Grano (2006)	1
Schubert (2008)	0.5	Changunda et al. (2008)	1
Jameson (2010)	0.75		

Table 4.3 shows that the typical values of N found in theoretical studies are in the range of 0.44 – 0.75. In experimental studies the values of N have been found to be in the range of 0.75 – 1, which is higher than the theory would suggest. The values of N found in the current study (0.7 and 0.9) are within the lower end of the range of values found in experimental studies, and are higher than would typically be expected from theory. This indicates that the dependence of flotation rate on energy dissipation is possibly stronger than theory suggests, however it may not be as strong as some experimental studies have found.

Previous work in an oscillating grid cell was conducted by Changunda et al. (2008) at energy dissipations of 0.015 – 0.60 kW/m^3. For the range of energy dissipations used, the value of N was found to be 1, and it was proposed that the effect that energy dissipation has on the flotation rate is not strongly dependent on the bubble size (see Section 2.5.3.3). Figure 4.13 shows that, when investigating an extended range of higher energy dissipations (0.5 – 5 kW/m^3), the dependence of flotation rate on energy dissipation is not as strong as suggested by Changunda et al. (2008), and the effect of energy dissipation on flotation rate is dependent on the bubble size.

4.3 The Effect of Contacting Environment on Flotation Kinetics

The majority of literature flotation studies have been conducted in stirred cells, which are considered to have contacting environments that are not well suited to investigating the effect of energy dissipation on flotation kinetics. Novel cells, which potentially provide more ideal contacting environments for the investigation of energy dissipation on flotation kinetics, have therefore been developed. Two such cells are the oscillatory baffled column (Anderson, 2008) and the oscillating grid cell (Changunda et al., 2008). This section investigates the effect that contacting environment has on flotation kinetics, and how flotation in the more ideal oscillating grid cell compares to the traditional stirred cell.

In order to discuss the effect of the contacting environment on flotation performance, the results from quartz flotation in a stirred cell (Deglon, 1998), an oscillatory baffled column (Anderson, 2008), and the oscillating grid cell (current study) are compared

in Figure 4.14. In order to compare the flotation rates they have been normalised by dividing by the flotation rate at 0.5 kW/m^3 for the stirred cell and oscillating grid cell, and by the rate with no energy dissipation for the oscillatory baffled column. The flotation in the oscillating grid cell and oscillatory baffled column was performed using quartz of similar size range and hydrophobicity, whilst the flotation in the stirred cell was conducted using relatively less hydrophobic quartz. The bubble size used in the oscillatory baffled column was 0.65 mm, whilst 0.82 mm bubbles were used in the oscillating grid cell and the stirred cell.

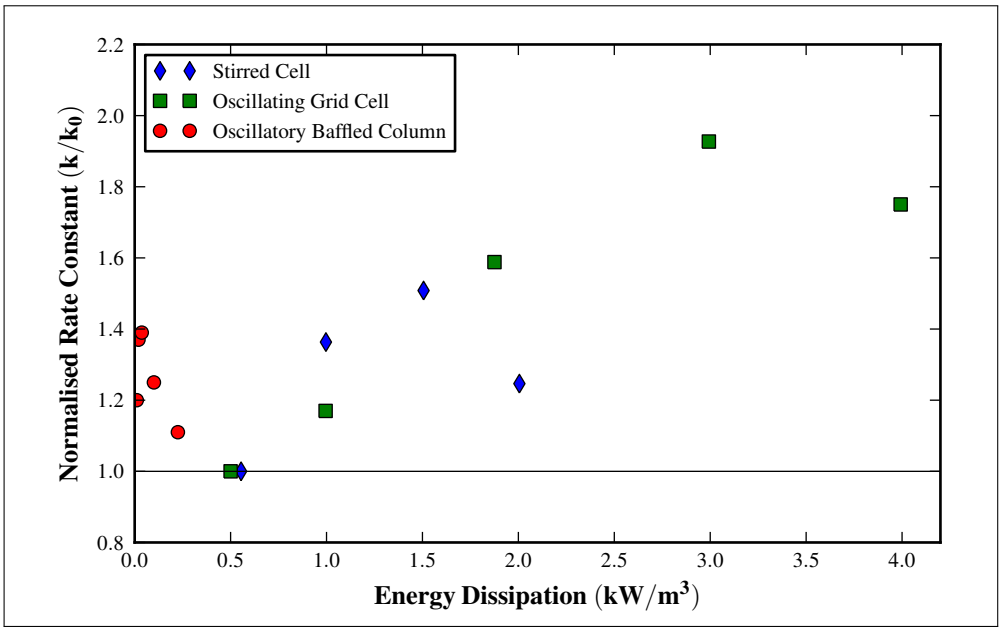

Figure 4.14: Flotation rate constant of quartz versus energy dissipation in an oscillatory baffled column (Anderson, 2008), an impeller stirred cell (Deglon, 1998) and an oscillating grid cell.

Figure 4.14 illustrates that for the three cells the flotation rates increased initially with increasing energy dissipation to an optimum, after which the flotation rate decreased. This optimum energy dissipation occurred at 0.05 kW/m^3 for the oscillatory baffled column, 1.5 kW/m^3 for the stirred cell, and 3 kW/m^3 for the oscillating grid cell. This result indicates that the oscillatory baffled column exhibits flotation characteristics which differ greatly from the stirred cell and the oscillating grid cell, with the flotation rates being strongly influenced at low energy dissipations. Anderson (2008) proposed that the strong effect of energy dissipation on flotation rates, in the

oscillatory baffled column, arose from the additional oscillatory flow of the fluid in the system. This leads to an "apparent" fluctuating velocity of bubbles and particles at relatively low energy dissipation. Since it is thought to be the fluctuating velocity which is responsible for particle-bubble collisions in turbulent systems, this additional fluctuating velocity present in the oscillatory baffled column leads to increased collision rates. Additionally it leads to increased detachment at low energy dissipation. The oscillatory baffled column is therefore an energy efficient cell, but is not suitable for investigating the effect of energy dissipation on flotation kinetics.

The flotation characteristics of the stirred cell and oscillating grid cell are relatively closely matched at low energy dissipation. At increased energy dissipation above 1.5 kW/m^3 the flotation rates for the stirred cell decreased, whilst the flotation rates in the oscillating grid increased. This difference may be due to the high energy dissipation rates in the impeller zone of the stirred cell resulting in increased detachment rates in the system.

The oscillating grid cell can be considered to be a suitable tool for the investigation of the effect of energy dissipation on flotation kinetics. This is due to the fact that it operates over the same range of energy dissipations as a stirred cell, whilst generating more uniform and near ideal turbulence than found in stirred cells. It has been found that the results from stirred cells and the oscillating grid cell are comparable at low energy dissipations, however at higher energy dissipations it appears that high detachment rates near the impeller begin to dominate. The results in this study for the effect of energy dissipation on flotation kinetics, as presented in Section 4.2.2, may therefore be considered to be a more accurate representation than experimental studies conducted in stirred cells.

Chapter 5

Conclusions

The aim of this study was to investigate the effect of energy dissipation on flotation kinetics in an ideal turbulent environment. This was achieved by using an oscillating grid cell, which is a cell that was developed by Changunda et al. (2008) as a flotation device that generates a near ideal turbulent environment. For this investigation a new oscillating grid cell was built which operates at a large range of energy dissipations of 0.5 – 5 kW/m^3. The conclusions made from this investigation are presented in terms of the use of the oscillating grid cell as an experimental flotation device, and the observed effects of energy dissipation on flotation kinetics in the oscillating grid cell.

5.1 The Oscillating Grid Cell

The oscillating grid cell is considered to generate nearly isotropic and homogeneous turbulence, whilst decoupling the processes of turbulence generation, particle suspension and bubble break-up. This is thought to be a near ideal contacting environment in which to investigate flotation, which cannot be achieved in standard stirred cells.

Flotation experiments in the oscillating grid cell investigated the effects of particle size, bubble size and energy dissipation on the flotation rate of quartz. Results show that there is good agreement between flotation in the oscillating grid cell and findings in the literature for experimental studies using stirred cells. Additionally the oscillating grid cell operates in a similar range of energy dissipations to stirred cells.

The oscillating grid cell is therefore considered to be an ideal experimental tool for investigating the effect of energy dissipation on flotation kinetics, since it has similar flotation behaviour and operates over the same range of energy dissipations as a stirred cell, whilst generating more uniform and near ideal turbulence. Results for the effect of energy dissipation on flotation rate from this study may be considered to be a more accurate representation than experimental studies conducted in stirred cells, due to the more homogeneous environment that the oscillating grid cell provides.

5.2 The Effect of Energy Dissipation on Flotation Kinetics

Flotation experiments were conducted in the oscillating grid cell, for the flotation of quartz at energy dissipations of 0.5 – 5 kW/m^3 and bubbles sizes of 0.13 mm, 0.24 mm and 0.82 mm. The results from the experiments allow the following conclusions, regarding the effect of energy dissipation on flotation kinetics, to be made:

- The optimum flotation conditions, for all particle sizes, are fine bubbles and low energy dissipations. When floating with fine bubbles there is no benefit to increasing the energy dissipation.
- For flotation using larger bubbles, closer to those typically used in industry, increasing the energy dissipation is beneficial for the flotation of intermediate and fine particles. For more coarse particles it is beneficial to an optimum point, beyond which increasing energy dissipation results in decreased flotation rates. The value of this optimum energy dissipation for flotation decreases with decreasing bubble size.
- It has been proposed that detachment rates increase with increasing energy dissipation, increasing particle size and decreasing bubble size.
- The relationship between flotation rate and energy dissipation, in conditions where detachment is thought to be negligible, can be described by the relationship $k \propto \epsilon^{0.7-0.9}$. This relationship is stronger than theory would suggest, and

is in agreement with literature experimental studies which have made similar observations.

- Comparison between the results from the current investigation, and results from literature studies using an oscillatory baffled column (Anderson, 2008) and a stirred cell (Deglon, 1998), showed that the effect that energy dissipation has on flotation kinetics is dependent on the contacting environment.
- It has been found that the results from stirred cells and the oscillating grid cell are comparable at low energy dissipations, however in stirred cells at higher energy dissipations it appears that high detachment rates near the impeller begin to dominate.

5.3 Recommendations for Future Work

The results from the study have potential applications in the design and operation of industrial cells, and some suggestions can be made for future work in this area. In industrial cells the energy dissipation is non-homogeneous, and the results from the current study might not be directly applicable. It is proposed that CFD (computational fluid dynamics) simulations of the energy dissipation distribution in industrial cells may be used, in conjunction with flotation rate data from experiments in the oscillating grid cell, to estimate the flotation performance of a cell. Using such a method various cell designs may be investigated and evaluated.

References

Abrahamson, J., 1975. Collision rates of small particles in a vigorously turbulent fluid. Chemical Engineering Science 30 (11), 1371 – 1379.

Ahmed, N., Jameson, G., 1985. The effect of bubble-size on the rate of flotation of fine particles. International Journal of Mineral Processing 14 (3), 195–215.

Ahmed, N., Jameson, G., 1989. Flotation kinetics. Mineral Processing and Extractive Metallurgy Review 5, 77–99.

Anderson, C. J., 2008. Flotation in a novel oscillatory baffled column. Ph.D. thesis, University of Cape Town, Department of Chemical Engineering, Cape Town.

Anfruns, J. P., Kitchener, J. A., 1977. Rate of capture of small particles in flotation. Transactions of the Institution of Mining and Metallurgy, Section C Mineral Processing and Extractive Metallurgy 86, C9–C19.

Bache, D. H., Rasool, E., 1996. Measurement of the rate of energy dissipation around an oscillating grid by an energy balance approach. The Chemical Engineering Journal and the Biochemical Engineering Journal 63, 105–115.

Bache, D. H., Rasool, E., 2001. Characteristics of turbulence in a multigrid mixer. Chemical Engineering Journal 83, 67–78.

Batchelor, G. K., 1951. Pressure fluctuations in isotropic turbulence. Proceedings of the Cambridge Philosophical Society 47, 359–374.

Bergh, L., Yianatos, J., 2003. Flotation column automation: state of the art. Control Engineering Practice 11 (1), 67–72.

Brady, M. R., Telionis, D. P., Vlachos, P. P., Yoon, R.-H., 2006. Evaluation of multiphase flotation models in grid turbulence via particle image velocimetry. International Journal of Mineral Processing 80 (2-4), 133 – 143.

Breytenbach, J. N., 1995. An investigation of particle collection efficiency in different particle-bubble contacting environments in flotation. Master's thesis, University of Cape Town, Department of Chemical Engineering, Cape Town.

Brunk, B. K., Koch, D. L., Lion, L. W., 1998. Observations of coagulation in isotropic turbulence. Journal of Fluid Mechanics 371, 81–107.

Camp, T. R., Stein, P. C., 1943. Velocity gradients and internal work in fluid motion. Journal of the Boston Society of Civil Engineers 30(4), 219–237.

Changunda, K., Harris, M., Deglon, D. A., 11 2008. Investigating the effect of energy input on flotation kinetics in an oscillating grid flotation cell. Minerals Engineering 21 (12-14), 924–929.

Collins, G. L., Jameson, G. J., 1976. Experiments on the flotation of fine particles - the influence of particle size and charge. Chemical Engineering Science 3, 985–991.

Crawford, R., Ralston, J., 1988. The influence of particle size and contact angle in mineral flotation. International Journal of Mineral Processing 23, 1–24.

Dai, Z., Dukhin, S., Fornasiero, D., Ralston, J., 1998. The inertial hydrodynamic interaction of particles and rising bubbles with mobile surfaces. Journal of Colloid and Interface Science 197 (2), 275 – 292.

Dai, Z., Fornasiero, D., Ralston, J., 1999. Particle-bubble attachment in mineral flotation. Journal of Colloid and Interface Science 217 (1), 70 – 76.

De-Silva, I. P. D., Fernando, H. J. S., 1994. Oscillating grids as a source of nearly isotropic turbulence. Physics of Fluids 6 (7), 2455–2464.

Deglon, D., 2002. A novel attachment - detachment kinetic model. In: Flotation and Flocculation - From Fundamentals to Applications. Hawaii.

Deglon, D., Egya-mensah, D., Franzidis, J., 2000. Review of hydrodynamics and gas dispersion in flotation cells on south african platinum concentrators. Minerals Engineering 13 (3), 235 – 244.

Deglon, D. A., 1998. A hydrodynamic investigation of fine particle flotation in a batch flotation cell. Ph.D. thesis, University of Cape Town, Department of Chemical Engineering, Cape Town.

Diaz-Penafiel, P., Dobby, G., 1994. Kinetic studies in flotation columns: Bubble size effect. Minerals Engineering 7 (4), 465 – 478.

Dobby, G. S., Finch, J. A., 1986. A model of particle sliding time for flotation size bubbles. Journal of Colloid and Interface Science 109 (2), 493–498.

Duan, J., Fornasiero, D., Ralston, J., 2003. Calculation of the flotation rate constant of chalcopyrite particles in an ore. International Journal of Mineral Processing 72 (1-4), 227 – 237, special Issue To Honor Professor Douglas W. Fuerstenau.

Evans, G., Doroodchi, E., Lane, G., Koh, P., Schwarz, M., 2008. Mixing and gas dispersion in mineral flotation cells. Chemical Engineering Research and Design 86 (12), 1350–1362, international Symposium on Mixing in Industrial Processes.

Finch, J. A., 1995. Column flotation: a selected review - part IV: novel flotation devices. Minerals Engineering 8 (6), 587–602.

Gaudin, A. M., 1957. Flotation, 2nd ed. McGraw Hill Book Co. Inc. New York.

Gaudin, A. M., R. Schuhmann, J., Schlechten, A. W., 1942. Flotation kinetics. II. The effect of size on the behavior of galena particles. The journal of physical chemistry 46, 902–910.

Guadayol, O., Peters, F., Stiansen, J. E., Marrase, C., Lohrmann, A., 2009. Evaluation of oscillating grids and orbital shakers as means to generate isotropic and homogeneous small-scale turbulence in laboratory enclosures commonly used in plankton studies. Limnology And Oceanography - Methods 7, 287–303.

Hopfinger, E., Toly, J., 1976. Spatially decaying turbulence and its relation to mixing across density interfaces. Journal Of Fluid Mechanics 78, 155.

Huppert, H. E., Turner, J. S., Hallworth, M. A., 1995. Sedimentation and entrainment in dense layers of suspended particles stirred by an oscillating grid. Journal of Fluid Mechanics 289, 263–293.

Ityokumbul, M. T., de Aquino, J. A., O'Connor, C. T., Harris, M. C., 2000. Fine pyrite flotation in an agitated column cell. International Journal of Mineral Processing 58 (1-4), 167 – 178.

Jameson, G., Nam, S., Young, M., 1977. Physical factors affecting recovery rates in flotation. Mineral Science Engineering 9, 103–118.

Jameson, G. J., 2010. New directions in flotation machine design. Minerals Engineering 23 (11-13), 835 – 841.

Jordan, C., Spears, D., 1990. Evaluation of a turbulent flow model for fine-bubble and fine-particle flotation. Mineral Processing and Extractive Metallurgy Review 7, 65 – 73.

Julien Saint Amand, F., 1999. Hydrodynamics of de-inking flotation. International Journal of Mineral Processing 56 (1-4), 277 – 316.

Koh, P., Schwarz, M., 2006. CFD modelling of bubble-particle attachments in flotation cells. Minerals Engineering 19 (6-8), 619 – 626, selected papers from the Centenary of Flotation Symposium, 5-9 June 2005, Brisbane, Australia.

Koh, P. T. L., Schwarz, M. P., 2003. CFD modelling of bubble-particle collision rates and efficiencies in a flotation cell. Minerals Engineering 16 (11), 1055 – 1059.

Kolmogorov, A. N., 1941. Dissipation of energy in a locally isotropic turbulence. Doklady Akad. Nauk SSR 32, 141, in Nguyen and Schulze (2004). *op cit.*

Lee, C. H., Erickson, L. E., 1987. Bubble breakup and coalescence in turbulent gas-liquid dispersions. Chemical Engineering Communications 59(1-6), 65–84.

Lelinski, D., Govender, D., Dabrowski, B., Traczyk, F., Mulligan, M., 2011. Effective use of energy in the flotation process. In: The Southern African Institute of Mining and Metallurgy 6th Southern African Base Metals Conference.

Liem, L. E., Smith, D. W., Stanley, S. J., March 1999. Turbulent velocity in flocculation by means of grids. Journal of Environmental Engineering 125 (3), 224–233.

Liepe, F., Mockel, H.-O., 1976. Untersuchungen zum stoffvererinigen in flussiger phase. Chem. Techn. 23, 231, in Schulze (1977). *op cit.*

Mao, L., Yoon, R.-H., 1997. Predicting flotation rates using a rate equation derived from first principles. International Journal of Mineral Processing 51 (1-4), 171 – 181, application of Surface Science to Advancing Flotation Technology.

McDougall, T. J., 1979. Measurements of turbulence in a zero-mean-shear mixed layer. Journal of Fluid Mechanics 94, 409–431.

McKenna, S. P., McGillis, W. R., 2004. Observations of flow repeatability and secondary circulation in an oscillating grid-stirred tank. Physics of Fluids 16 (9), 3499 – 3502.

Miettinen, T., Ralston, J., Fornasiero, D., 2010. The limits of fine particle flotation. Minerals Engineering 23, 420 – 437.

Mokgethi, B., 2010. The effect of energy input on precipitation in an oscillating grid reactor. Master's thesis, University of Cape Town, Department of Chemical Engineering, Cape Town.

Newell, R., Grano, S., 2006. Hydrodynamics and scale up in rushton turbine flotation cells: Part 2 – flotation scale-up for laboratory and pilot cells. International Journal of Mineral Processing 81, 65–78.

Newell, R., Grano, S., 2007. Hydrodynamics and scale up in rushton turbine flotation cells: Part 1 – cell hydrodynamics. International Journal of Mineral Processing 81 (4), 224 – 236.

Nguyen, A., Schulze, H., 2004. Colloidial Science of Flotation. Vol. 118 of Surfactant Science Series. Marcel Dekker, Inc.

Nonaka, M., Inoue, T., Imaizumi, T., 1982. A micro-hydrodynamic flotation model and its application to the flotation process. In: Proceedings XIV International Mineral Processing Congress, Toronto.

Orlins, J., Gulliver, J., 2003. Turbulence quantification and sediment resuspension in an oscillating grid chamber. Experiments in Fluids 34, 662 – 677.

Pyke, B., 2004. Bubble-particle capture in turbulent flotation systems. Ph.D. thesis, University of South Australia, Ian Wark Research Institute.

Pyke, B., Fornasiero, D., Ralston, J., 2003. Bubble particle heterocoagulation under turbulent conditions. Journal of Colloid and Interface Science 265, 141 – 151.

Ralston, J., Fornasiero, D., Hayes, R., 1999. Bubble-particle attachment and detachment in flotation. International Journal of Mineral Processing 56 (1-4), 133 – 164.

Reay, D., Ratcliff, G. A., 1975. Experimental testing of the hydrodynamic collision model of fine particle flotation. The Canadian Journal of Chemical Engineering 53, 481–486.

Rodrigues, R. T., Rubio, J., 2007. DAF-dissolved air flotation: Potential applications in the mining and mineral processing industry. International Journal of Mineral Processing 82 (1), 1 – 13.

Saffman, P., Turner, T., 1956. On the collision of drops in turbulent clouds. Journal of Fluid Mechanics 1, 16–30.

Schubert, H., 1999. On the turbulence-controlled microprocesses in flotation machines. International Journal of Mineral Processing 56 (1-4), 257 – 276.

Schubert, H., 2008. On the optimization of hydrodynamics in fine particle flotation. Minerals Engineering 21 (12-14), 930 – 936, selected Papers from Flotation '07.

Schulze, H., 1977. New theoretical and experimental investigations on stability of bubble/particle aggregates in flotation: a theory on the upper particle size of floatability. International Journal of Mineral Processing 4, 241–259.

Schulze, H., 1982. Dimensionless number and approximate calculation of the upper particle size of floatability in flotation machines. International Journal of Mineral Processing 9, 321–328.

Sherrell, I. M., 2004. Development of a flotation rate equation from first principles under turbulent flow conditions. Ph.D. thesis, Virginia Polytechnic Institute and State University, Blacksburg, Virginia.

Shy, S. S., Tang, C. Y., Fann, S. Y., 1997. A nearly isotropic turbulence generated by a pair of vibrating grids. Experimental Thermal and Fluid Science 14 (3), 251–262.

Srdic, A., Fernando, H., Montenegro, L., 1996. Generation of nearly isotropic turbulence using two oscillating grids. Experiments in Fluids 20 (5), 395–397.

Sutherland, K., 1948. Kinetics of the flotation process. Journal of Physical and Colloidal Chemistry 52, 394 – 425.

Tojo, K., Miyanami, K., Minami, I., Yano, T., 1979. Power dissipation in a vibrating disc column. Chemical Engineering Journal and the Biochemical Engineering Journal 17 (3), 211–218.

Trahar, W., 1981. A rational interpretation of the role of particle size in flotation. International Journal of Mineral Processing 8 (4), 289–327.

Villermaux, E., Sixou, B., Gagne, Y., 1995. Intense vortical structures in grid-generated turbulence. Physics of Fluids 7 (8), 2008.

Yan, J., Cheng, N.-S., Tang, H.-W., Tan, S. K., 2007. Oscillating-grid turbulence and its applications: a review. Journal of Hydraulic Research 45 (1), 26–32.

Yianatos, J., Henrquez, F., Tapia, L., 2008. Evaluation of the largest flotation cells at Minera Los Pelambres. Minerals Engineering 21 (12-14), 841 – 845, selected Papers from Flotation 07.

Yoon, R., Luttrell, G., 1986. The effect of bubble size on fine coal flotation. Coal Preparation 2, 179–192.

Yoon, R., Luttrell, G., 1989. The effect of bubble size on fine particle flotation. Mineral Processing and Extractive Metallurgy Review 5, 101 – 122.

Yoon, R.-H., Mao, L., 1996. Application of extended DLVO theory, IV: Derivation of flotation rate equation from first principles. Journal of Colloid and Interface Science 181 (2), 613 – 626.

Appendix A: Flotation Data

A.1 Methylated Quartz Flotation Data

Table A.1: Flotation rates for methylated quartz floated at 0.5 kW/m^3.

Bubble Size	**Particle Size Class (μm)**		
(mm)	**-19 +5**	**-45 +19**	**-74 +45**
0.82	0.0171	0.0367	0.0687
0.24	0.0404	0.0849	0.1521
0.13	0.0553	0.1370	0.2258

A.2 Natural Quartz Flotation Data

Table A.2: Flotation rates for natural quartz flotation with 0.82 mm bubbles.

Energy Dissipation	**Particle Size Class (μm)**		
(kW/m^3)	**-19 +5**	**-45 +19**	**-74 +45**
0.5	0.0139	0.0393	0.0600
1	0.0189	0.0467	0.0702
2	0.0371	0.0747	0.0953
3	0.0553	0.0992	0.1157
4	0.0570	0.0956	0.1051
5	0.0660	0.1011	0.1010

Table A.3: Flotation rates for natural quartz flotation with 0.24 mm bubbles.

Energy Dissipation	**Particle Size Class (μm)**		
(kW/m^3)	**-19 +5**	**-45 +19**	**-74 +45**
0.5	0.0313	0.0637	0.0969
1	0.0365	0.0761	0.1156
2	0.0401	0.0827	0.1087
3	0.0554	0.0962	0.1057
4	0.0578	0.0935	0.0980
5	0.0679	0.0944	0.0893

Table A.4: Flotation rates for natural quartz flotation with 0.13 mm bubbles.

Energy Dissipation	**Particle Size Class (μm)**		
(kW/m^3)	**-19 +5**	**-45 +19**	**-74 +45**
0.5	0.0735	0.1350	0.1859
1	0.0726	0.1285	0.1763
2	0.0697	0.1221	0.1501
3	0.0598	0.0992	0.1124
4	0.0632	0.1024	0.1118
5	0.0644	0.0953	0.0946

Appendix B: Literature Data

Table B.1: Flotation rate data from Deglon (1998).

Experimental Conditions					
Cell Type	Rushton impeller agitated tank				
Cell Volume (L)	2.25				
Gas Flowrate (mL/min)	400				
Ore	Quartz				
Particle Size (μm)	sub 100				
Collector Type	HPYC				
Collector Dosage (ppm)	171				
Bubble Size (mm)	0.82				
Flotation Data					
Impeller Speed (RPM)	310	580	730	840	940
Energy Dissipation (kW/m^3)	0.096	0.554	0.996	1.505	2.005
Rate constant (s^{-1})	0.004	0.009	0.013	0.014	0.012

Table B.2: Flotation rate data from Anderson (2008).

Experimental Conditions						
Cell Type	Oscillatory baffled column					
Cell Volume (L)	13					
Gas Flowrate (L/min)	0.55					
Ore	Quartz					
Particle Size (μm)	36 – 76 μm					
Collector Type	Dodecylamine					
Collector Dosage (mol/L)	1×10^{-4}					
Bubble Size (mm)	0.65					
Amplitude of Oscillation (mm)	10					
Flotation Data						
Oscillating Frequency (Hz)	0	1.44	1.76	2.18	2.96	3.75
Energy Dissipation (kW/m^3)	0	0.01	0.019	0.036	0.100	0.225
Rate constant (min^{-1})	1.88	2.26	2.59	2.63	2.36	2.09